# Multiple combustion modes switching to realize full-load efficient operation of n-butanol/diesel dual direct injection ($DI^2$) engine

Yikang Cai [a], Ming Jia [a, *], Yaopeng Li [a], Antonio García [b], Javier Monsalve-Serrano [b]

[a] Key Laboratory of Ocean Energy Utilization and Energy Conservation of Ministry of Education, Dalian University of Technology, Dalian 116024, P.R. China

[b] CMT – Motores Térmicos, Universitat Politècnica de València, Camino de Vera s/n, 46022 Valencia, Spain

*Energy Conversion and Management*

*Volume 278, 15 February 2023, 116722*

## Abstract

The dual direct injection ($DI^2$) strategy is a novel combustion concept involving the in-cylinder co-direct injection of two fuels with the potential to operate in multiple combustion modes over a wide load range to achieve the practical applications of dual-fuel engines. However, for the $DI^2$ strategy, its optimal fuel organization under different loads is still unknown. Thus, by selecting n-butanol and diesel as the test fuels, this study aims to identify the optimal combustion mode of the $DI^2$ strategy at different load conditions using three-dimensional engine simulation combined with genetic algorithm. The results showed that for low load, the optimal $DI^2$ strategy is to pre-inject a low proportion of diesel (near 20%) into the cylinder early in the compression stroke and then introduce n-butanol into the diesel atmosphere. The late-injected n-butanol can increase the local equivalence ratio to avoid overly lean fuel/air mixture while the pre-injected diesel can increase the in-cylinder fuel chemical reactivity and assist ignition, thereby improving the combustion efficiency at low load conditions. On the contrary, the fuel injection sequence is reversed at mid load, in which n-butanol is first injected into the combustion chamber to form a partially premixed n-butanol/air mixture, followed by a late diesel injection at -50 to -20 °CA after top dead center (TDC). Because a large amount of n-butanol is partially premixed in advance under mid load, the homogeneity of the mixture is promoted, which improves fuel economy and reduces nitrogen oxides ($NO_x$) formation. As for the high-load operation, n-butanol is still preferred to be partially premixed, but the diesel injection event is delayed until after TDC. The diesel injection after TDC helps to increase the engine power output and reduce the fuel reactivity during the auto-ignition to avoid premature combustion and high pressure rise rate issues. The main factors driving the ignition under low load are the fuel reactivity and temperature, while at mid load the ignition is primarily initiated by fuel reactivity, however, the effect of temperature is highlighted under high load.

**Keywords**: Dual direct injection ($DI^2$); Multi-load optimization; Multiple combustion modes; Ignition mechanism

# 1. Introduction

The global energy shortage and environmental pollution have impelled the engine community to seek efficient combustion strategies and clean fuel sources. Butanol, as an oxygenated biofuel, has received special attention from researchers in recent years considering its distinctive fuel properties and improved yields. Butanol can be produced from various biomass (e.g., starch-rich crops and lignocellulose) by biological fermentation, like the commonly used acetone-butanol-ethanol (ABE) process [1]. Benefiting from innovative production technologies, the productivity of butanol has been significantly enhanced [2–5]. Compared to short-chain alcohols, such as methanol and ethanol, butanol owns higher energy density, lower latent heat of vaporization, higher viscosity, lower corrosion, and better miscibility, etc., which make it a better choice when used in engines [6]. According to the different molecular structures, butanol can be classified as four isomers, namely n-butanol, sec-butanol, iso-butanol, and tert-butanol. For the butanol extracted from biomass (biobutanol), a straight-chain structure is usually obtained, known as n-butanol, which shows the fastest burning velocity among the four isomers and has been extensively investigated as a potential future fuel in diesel engines.

Recently, growing studies on n-butanol-relevant combustion strategies have been reported. Zheng et al. [7,8], for example, confirmed the feasibility of port fuel injection (PFI) or direct injection (DI) of neat n-butanol for achieving high thermal efficiency and ultra-low nitrogen oxides ($NO_x$) and soot emissions based on a light-duty diesel engine. Despite these demonstrated benefits, high unburned hydrocarbon (UHC) and carbon monoxide (CO) were found for neat n-butanol combustion, and its practical operating range was also confined to low-to-mid loads due to fast heat release rate and uncontrollable ignition timing and combustion phasing in compression-ignition engines. The n-butanol directly blended with diesel is another common way to make n-butanol available in existing diesel engines. The previous research [9–11] related to n-butanol/diesel blends indicated that blending n-butanol into diesel can accelerate combustion rate and extend ignition delay to enhance premixed combustion and then improve brake thermal efficiency. Also, because of the oxygen-containing nature of n-butanol, the engine-out soot emissions can be dramatically reduced. However, hydrocarbon emissions tend to increase for higher n-butanol blending ratios, especially at low-load conditions, which is due to the higher heat of evaporation of the blends, enhanced spray-wall interaction, and larger lean flame-out zones [11]. Moreover, although n-butanol has better miscibility with diesel fuel due to its lower polarity as compared to methanol and ethanol, the maximum n-butanol ratio of blends is generally limited below 40% (by volume) to keep appropriate cetane number and lubricity [12]. Therefore, considering the inherent defects of neat n-butanol and n-butanol/diesel blends fueled engines, one effective way to enhance the full-load operation capability of n-butanol engines and avoid the limitations on n-butanol blending ratio is to use n-butanol and diesel fuels simultaneously in an in-direct blending manner, typically including reactivity controlled compression ignition (RCCI) strategy and dual direct injection ($DI^2$) strategy.

The RCCI is a well-studied combustion concept involving the use of two reactivity fuels with distinct auto-ignition abilities, such as gasoline/diesel [13,14], methanol/diesel [15,16], butanol/diesel [17,18], syngas/diesel [19,20], etc., where the low-reactivity fuel (LRF) is usually premixed through PFI, and the high-reactivity fuel (HRF) is directly injected into the virtually homogeneous low-reactivity fuel atmosphere to initiate ignition and control the heat release process. In RCCI, the combustion develops along the gradient of the high-reactivity fuel. With respect to the temperature and equivalence ratio stratifications, the fuel reactivity stratification is more important to the initial ignition process [21]. The gasoline/diesel RCCI experiments by Kokjohn et al. [22] indicated that by using this dual-fuel strategy, a gross indicated efficiency exceeding 50% at the mid-load point can be achieved while maintaining near-zero $NO_x$ and soot emissions. Although RCCI exhibits obviously enhanced thermal efficiency advantages, it usually yields high HC and CO emissions in squish regions near the liner due to the low cylinder wall temperature and the lean premixed fuel trapped in the crevice [23,24], in particular for low-load situations. Additionally, under high-load conditions, because a high proportion of low reactivity fuel is premixed in RCCI, it is difficult to control the reaction progress of the premixed mixture, and therefore suffers an unacceptable noise level. Both issues restrict the full-load operation capability of RCCI. It can therefore be inferred that in order to achieve efficient dual-fuel engine operation at different loads, the in-cylinder stratification level for both LRF and HRF may need to be adjusted individually in a wide range to meet the charge requirements of various operating conditions.

Concerning the above challenges raised by RCCI, a novel combustion concept, the dual direct injection ($DI^2$) strategy has been developed to address its high- and low-load dilemma, in which two fuels with different reactivity are directly injected into the cylinder at the designed timings. Currently, for the dual direct injection combustion concept, some specific implementations have been proposed, such as direct dual fuel stratification (DDFS) [25], intelligent charge compression ignition (ICCI), and dual fuel co-direct injection ($DI^2$) [26], all of which share the core idea of dual-fuel direct in-cylinder stratification through two independent fuel systems, and only fuel direct injection timings and injection fractions are different. Thus, in this study, different dual direct injection strategies are not specially distinguished, and all are denoted as $DI^2$. Previous work of comparing the n-butanol/diesel RCCI and $DI^2$ strategies under mid load by the authors [27] confirmed that the in-situ fuel mixing of the low-reactivity n-butanol in $DI^2$ is beneficial to reducing the incomplete oxidation within the near-liner area, resulting in decreased HC and CO emissions. Meanwhile, due to the more stratified in-cylinder charge, $DI^2$ exhibits lower combustion noise with the ability to be applied in a higher load. In the load extension study by Lim et al. [28], it was found that gross indicated mean effective pressure ($IMEP_g$) up to 21 bar can be achieved using the gasoline and diesel dual fuel direct injection strategy. More recently, Florea [26] and Neely et al. [29] conducted a series of engine experiments to examine the operating potential of the natural gas (NG) and diesel $DI^2$ strategy. The results indicated that the $DI^2$ strategy can enhance combustion efficiency and reduce methane emissions compared with the NG/diesel RCCI combustion, whereas the degree of methane reduction is highly dependent on the spray angle of NG.

More information on the comparison of the two strategies can also be found in Refs. [30,31]. In general, compared with RCCI, $DI^2$ presents significant advantages in improving combustion efficiency and expanding engine loads, promising to realize the full-load efficient operation of dual-fuel engines. In the $DI^2$ system, the reactivity and concentration stratifications of the mixture charge in the cylinder are fully decoupled because of independent dual fuel injection events, i.e., the fuel gradients and their spatial distributions can be independently controlled. For a specific operating condition, through adjusting the dual fuel introduced sequence, injection timings, and dual fuel split ratio, $DI^2$ can theoretically formulate the in-cylinder charge with desired stratification states in real time to achieve highly efficient engine combustion in this scenario. Therefore, for $DI^2$ engines, because of the more flexible fuel/air mixture preparation, it is potential to be operated with multiple combustion modes to obtain the optimal engine performance across the whole engine map.

The operation of $DI^2$ engines involves a number of control parameters, including the injection timings, injection pressure, and spray angles of LRF and HRF, dual fuel split ratio, as well as initial intake conditions (i.e., intake pressure, temperature, and exhaust gas recirculation (EGR) rate), that require to be optimized to improve the in-cylinder combustion process and engine performance before practical applications. However, the determination of the parameters in previous $DI^2$ studies is usually empirical. Although $DI^2$ retains the ability to be operated in multiple modes over a wide load range, much research effort about $DI^2$ mainly focused on a selected operating point and did not identify its optimal combustion mode under different loads. Moreover, the stratification features and the major factors driving the ignition of $DI^2$ at different optimal modes also need to be further summarized.

Considering the above research gaps, the main aim of this paper is to identify the optimal combustion modes of $DI^2$ at different engine loads using three-dimensional (3D) engine simulation combined with an improved non-dominated sorting genetic algorithm (NSGA-II) [32] and to reveal the inherent reasons for the multi-mode transition under different loads. The present work utilizes n-butanol and diesel as the test fuels, and the research content can be described as follows. First, three typical load points of 4, 7, and 14 bar IMEP corresponding to low, mid, and high loads, are selected to perform the full-parameter optimization of the n-butanol/diesel $DI^2$ strategy, thereby determining its best fuel organization and stratification state at different loads. Subsequently, based on the optimal fuel strategies, the effect of the dual fuel injection sequence on the combustion and emissions of $DI^2$ is detailed. Moreover, the impact of the crucial fuel injection parameters identified at different loads on the performance and emission formations of $DI^2$ is further analyzed. Finally, the key factors driving the ignition at each load are also analyzed.

# 2. Computational approach

The present investigation used an open-source 3D computational fluid dynamic (CFD) code, KIVA-3V [33], to simulate the spray, combustion, and emissions of the n-butanol/diesel $DI^2$ strategy and to determine its optimal fuel organization under different loads. The high fidelity of the simulation results depends on accurate flow, spray, heat transfer, and chemistry sub-models, therefore, some original sub-models in KIVA-3V have been further enhanced. A new generalized re-normalization group (gRNG) $k$-$\varepsilon$ turbulence model [34] was used to predict the complex turbulent transport process in engines, in which the flow anisotropy effects were introduced using the model coefficients that are a function of flow strain rate. The fuel spray modelling method used here is based on the Lagrangian-Eulerian framework, where the liquid phase is treated as Lagrangian fuel parcels, and the gas phase is resolved as continuous Eulerian fluid. Following this approach, several physical-based spray sub-models were used to further describe the spray-relevant evolution processes. The Kelvin–Helmholtz Rayleigh–Taylor (KH-RT) model [35] was used for the spray atomization and breakup simulation, and a new hybrid stochastic/trajectory (HST) model proposed by Suo et al. [36] was employed to reproduce droplet collision behavior, which has shown lower grid-size sensitivity and better predictions over spray macro-morphology and droplet size distributions under strong interaction of consecutive injection jets than previous collision models. The quasi-dimensional vaporization model proposed by Yi et al. was used to reproduce the vaporization process of multi-component droplets [37]. Moreover, considering the strong interaction of fuel sprays with the combustion chamber or cylinder wall in the dual fuel $DI^2$ system, an enhanced spray/wall interaction model [38] and an updated liquid film model proposed by Zhang et al. [39] were also applied. For the engine heat transfer calculation, the steady-state heat transfer model of Cao et al. [40] was employed to improve the prediction accuracy of wall heat flux under various combustion modes.

In the KIVA3V code, CHEMKIN [41] solver was integrated to calculate the fuel chemical reaction process without considering the sub-grid turbulence-chemistry interaction, i.e., each computational cell was modelled as a perfectly stirred reactor (PSR), which was successfully validated in earlier engine simulation studies for premixed or partially premixed combustion [22,42]. During the engine simulation, the realistic physical properties of n-butanol were used to calculate its non-chemical related processes, while for diesel fuel its physical characteristics were surrogated by n-dodecane, as used in Ref. [43]. The chemical model used here is the combined reduced mechanisms for n-butanol [44] and n-heptane [45] constructed through the decoupling methodology [46], where a detailed $H_2/CO/C_1$ sub-mechanism and a reduced $C_2$–$C_3$ sub-mechanism are coupled with two skeletal fuel-specific sub-mechanisms, i.e., the skeletal $C_4$ sub-mechanism for n-butanol and the skeletal $C_4$–$C_7$ sub-mechanism for n-heptane.

The $NO_x$ and soot emissions utilized in this study were respectively predicted using an extended Zeldovich $NO_x$ mechanism and an improved phenomenological soot model [47].

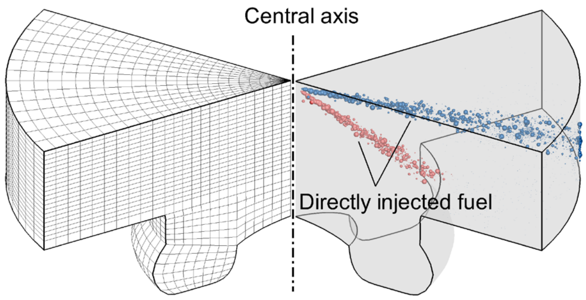


Fig. 1. Computational sector mesh and the fuel spray schematic diagram of $DI^2$ at -45 °CA ATDC.

The present study is conducted based on a light-duty Ford diesel engine with a high compression ratio of 18.2 and a re-entrant shaped piston bowl. The engine is operated at a constant speed of 1500 rev/min and has bore and stroke of 86 mm×86 mm. Furthermore, a 6-hole direct injector with a spray cone angle of 155° and nozzle hole diameter of 0.13 mm is used in the original engine. The intake valve closing (IVC) timing is set as -135.0 °CA after the top dead center (ATDC), and the exhaust valve opening (EVO) timing is 132 °CA ATDC. Fig. 1 illustrates the computational sector mesh used for the simulation at -45 °CA ATDC and the dual-fuel spray schematic diagram of $DI^2$. A 60° sector grid was used for simplicity, and both n-butanol and diesel injectors were assumed to be arranged coaxially at the center of the cylinder head with the same nozzle configuration but different injection parameters (injection timing, spray cone angle, and pressure) for both fuels. To achieve the co-direct injection of dual fuels, some concept- and product-level injectors were proposed and developed for various gas/liquid or liquid/liquid fuel combinations. Installing two independent injectors on the cylinder head is a common method to achieve the direct in-cylinder mixing of dual fuels [48–53], covering the fuel schemes such as gasoline/diesel, methanol/diesel, and hydrogen/diesel. In addition to using two injectors, the concentric-needle injector [54,55] from Westport Innovations

Inc. specially designed for liquefied nature gas (LNG) or hydrogen-based engines can also be used to realize the in-cylinder injection of gas/liquid dual fuels, where the liquid fuel needle is embedded inside the gas fuel needle to enable the separate control of dual fuel jets. For the liquid/liquid fuel scheme, the Wärtsilä twin needle injector [56] is a technically feasible solution to meet the requirements of the dual direct injection fuel system. Different from the embedded structure of the Westport injector needles, the two needle valves of the Wärtsilä injector are arranged side by side and very close to each other. Note that apart from the above available solutions, some conceptual designs of the co-direct injector used for the liquid/liquid dual fuel are also reported [57]. According to Lim [58], the coaxial design of injectors helps to reduce incomplete combustion and soot emissions. Moreover, in this paper, a single-shot injection was adapted for n-butanol and diesel, and their injection timings were limited after IVC to avoid extremely lean fuel-air mixture and high HC and CO emissions, i.e., just the closed-cycle period from IVC to EVO is modelled.

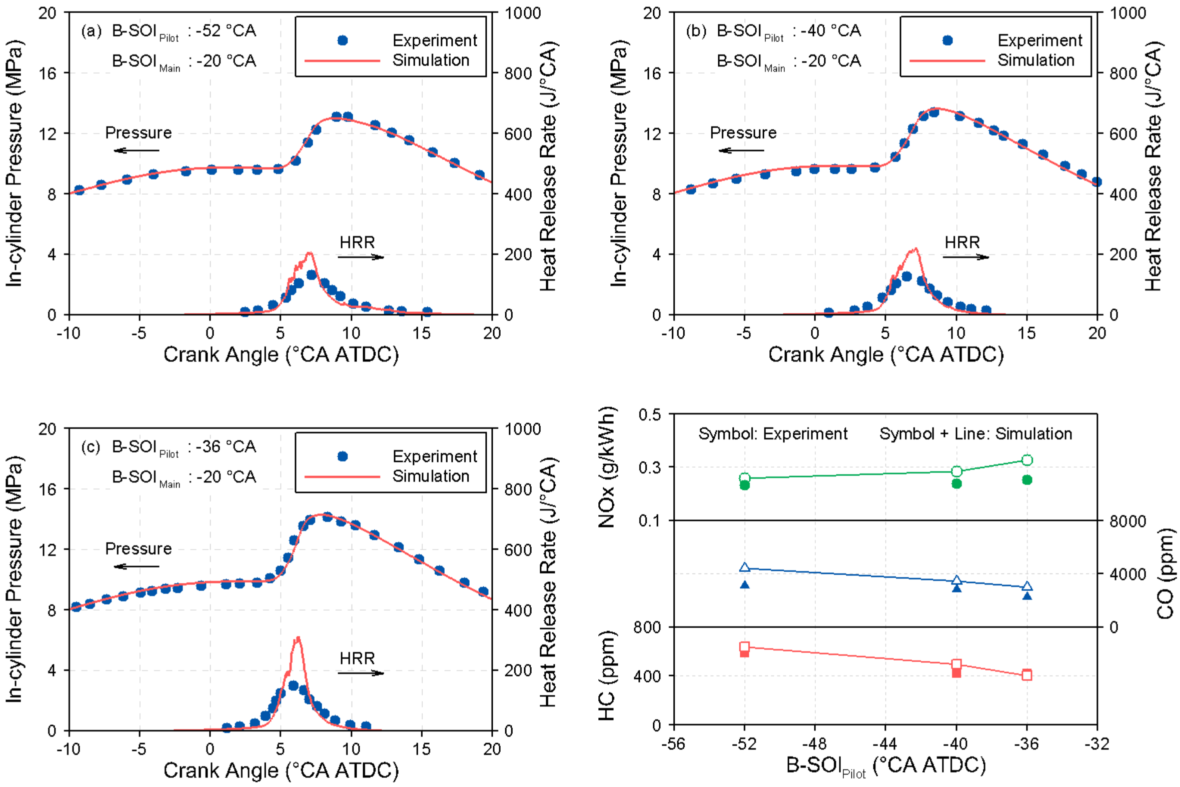


Fig. 2. Comparison of the in-cylinder pressure, heat release rate, HC, CO, and $NO_x$ emissions between experiment

[59] and simulation under the neat n-butanol pilot-injection strategy.

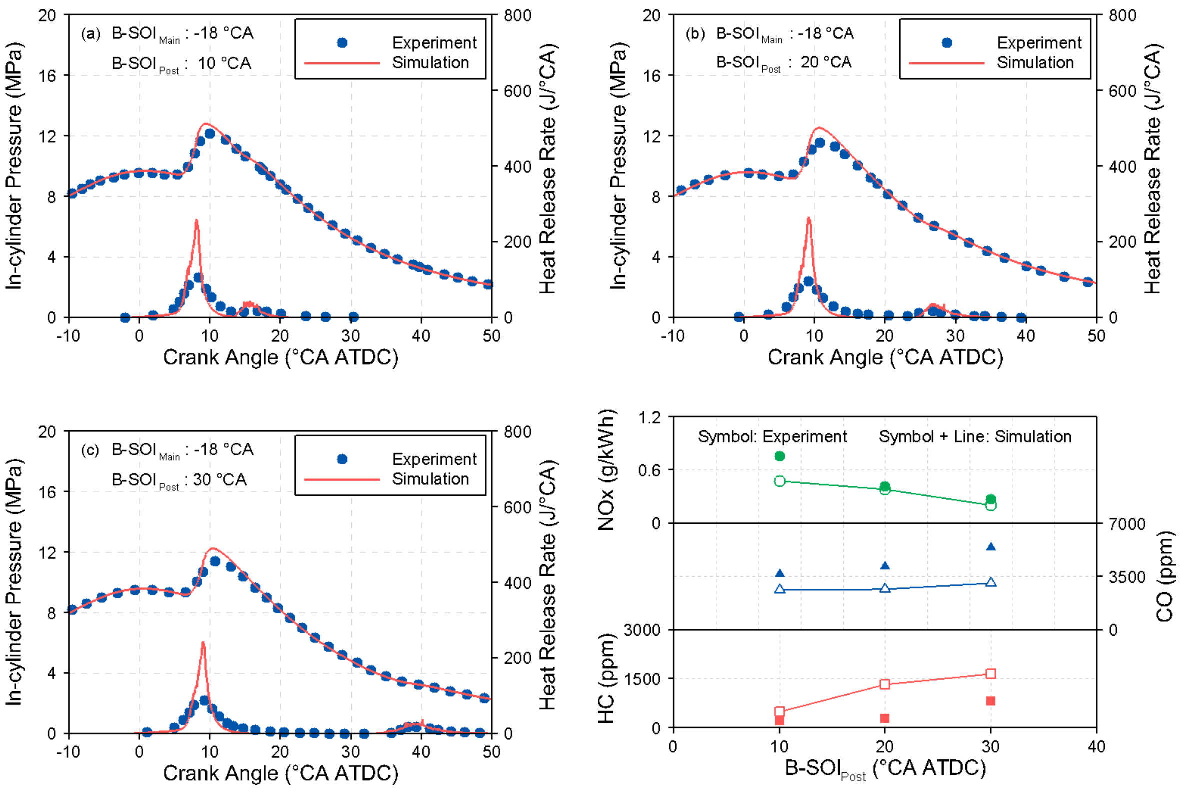


Fig. 3. Comparison of the in-cylinder pressure, heat release rate, HC, CO, and $NO_x$ emissions between experiment [59] and simulation under the neat n-butanol post-injection strategy.

The present numerical models have been extensively validated for various n-butanol and/or diesel low-temperature combustion (LTC) modes in the authors' previous work [27], and good agreements have been observed between experiments and measurements. In this paper, as a complement, based on the above test engine, the current models are validated against the available experimental data of the neat n-butanol with the pilot-injection strategy and the post-injection strategy from Jeftic et al [59]. In the pilot-injection strategy, the pilot-injection timing of n-butanol (B-SOI$_{Pilot}$) was varied from -52 to -36 °CA ATDC with a fixed injection duration of 300 µs (2.7 °CA), while the main injection timing (B-SOI$_{Main}$) of n-butanol was fixed at -20 °CA ATDC, and its duration was modulated to maintain a constant engine load of about 6 bar IMEP. Similarly, for the post-injection strategy, the post-injection timing of n-butanol (B-$SOI_{Post}$) was swept from 10 to 30 °CA ATDC using a constant injection duration of 330 μs (3.0 °CA), and its main injection timing (B-$SOI_{Main}$) was set at -18 °CA ATDC with also an adjustable duration to obtain the same load level as above. In both strategies, the injection pressure of n-butanol events was kept at 900 bar, and no intake heating, intake boost, and EGR were used in the engine tests. From the validation results shown in Figs. 2 and 3, it can be found that the simulated cylinder pressure and heat release rate (HRR) are in good agreement with the measured results, and the trend of emissions can also be well captured.

In the n-butanol/diesel $DI^2$ strategy, although the introduction of n-butanol-relevant injection variables, such as injection timing, spray angle, and injection pressure, provide higher freedom over the ignition and combustion control, it is difficult to determine the optimal parameter combination solely depending on the traditional calibration method due to numerous parameters and their strong coupling relationship. Thus, the KIVA-3V code was combined with the multi-objective genetic algorithm, NSGA-II, to decide the optimal fuel organization in $DI^2$ under low, mid, and high loads with the aim to achieve simultaneous optimization of equivalent indicated specific fuel consumption (EISFC), $NO_x$, and soot emissions in this work. The EISFC is used to evaluate the fuel economy of n-butanol/diesel dual fuel engine in this study, and it is calculated as:

$$\mathrm{ESIFC} = \frac{m_{\mathrm{diesel}} \cdot LHV_{\mathrm{diesel}} + m_{\mathrm{butanol}} \cdot LHV_{\mathrm{butanol}}}{LHV_{\mathrm{diesel}} \cdot \int_{\mathrm{IVC}}^{\mathrm{EVO}} p\mathrm{d}V} \tag{1}$$

where the $m_{\mathrm{diesel}}$ and $m_{\mathrm{butanol}}$ are respectively the directly injected diesel and n-butanol mass, and $LHV_{\mathrm{diesel}}$ and $LHV_{\mathrm{butanol}}$ are the lower heating value of the two fuels; $\int_{\mathrm{IVC}}^{\mathrm{EVO}} p\mathrm{d}V$ represents the indicated work calculated by integrating the in-cylinder pressure over volume from IVC to EVO. Furthermore, following the work of Eng [60], the ringing intensity (RI) is used to evaluate the knock level of the engine, and is defined as Eq. (2):

$$\mathrm{RI} \approx \frac{1}{2\gamma} \cdot \frac{\left(0.05 \cdot \left(\frac{\mathrm{d}p}{\mathrm{d}t}\right)_{\max}\right)^2}{p_{\max}} \cdot \sqrt{\gamma R T_{\max}} \tag{2}$$

where $p_{\max}$, $T_{\max}$, and $\left(\frac{\mathrm{d}p}{\mathrm{d}t}\right)_{\max}$ are respectively the peak value of the in-cylinder pressure, temperature, and pressure rise rate during the cycle; $\gamma$ and $R$ denote the ratio of specific heat and the universal gas constant, respectively.

In NSGA-II, to deal with the trade-off problem of multiple objectives, the concept of dominance is introduced. For individual $A$ and individual $B$, considering $n$ objectives, if $f_i(A) \leq f_i(B)$ and $f_i(A) < f_i(B)$ holds at least once, it is considered individual $A$ dominates $B$, where $i \in \{1 \ldots n\}$, and $f_i(A)$ and $f_i(B)$ represent the $i^{\text{th}}$ objectives of individuals $A$ and $B$. The set of all individuals non-dominated by other individuals is defined as the Pareto front, which exhibits the best performance on the objectives. Furthermore, the initial sampling process of NSGA-II was improved in this work, and the Sobol sequence method was used to replace the traditional random sampling method to enhance the global optimization ability of the algorithm in high-dimensional parameter space.

Table 1 Optimized parameter settings of $DI^2$ at different loads.

| Parameter | Low load /Mid load /High load |
|---|---|
| Energy per cycle | 420/780/1780 J/cyc |
| Initial pressure ($p_{IVC}$) | 1~3 bar |
| Initial temperature ($T_{IVC}$) | 340~420 K |
| EGR Rate | 0~1.0 |
| n-Butanol energy ratio ($R_b$) | 0~1.0 |
| n-Butanol SOI timing (B-SOI) | -135~30 °CA ATDC |
| Diesel SOI timing (D-SOI) | -135~30 °CA ATDC |
| n-Butanol injection pressure (B-$P_{Inj}$) | 30~150 MPa |
| Diesel injection pressure (D-$P_{Inj}$) | 30~150 MPa |
| n-Butanol spray angle (B-Angle) | 30~85° |
| Diesel spray angle (D-Angle) | 30~85° |

The parameters to be optimized for the n-butanol/diesel $DI^2$ strategy at different loads are shown in Table 1, including intake thermodynamic conditions (i.e., initial pressure ($p_{IVC}$) and temperature ($T_{IVC}$) at IVC, EGR rate) and dual fuel injection settings (i.e., start of injection of n-butanol (B-SOI), n-butanol injection pressure (B-$P_{Inj}$), n-butanol spray angle (B-Angle), start of injection of diesel (D-SOI), diesel injection pressure (D-$P_{Inj}$), diesel spray angle (D-

Angle), and n-butanol energy ratio ($R_b$) in the supplied fuel). The supplied total energy under different load conditions are kept at 420, 780, and 1780 J/cyc, corresponding to three typical engine loads of ~4 bar, ~7 bar, and ~14 bar IMEP, respectively. In the multi-load $DI^2$ optimization, the number of individuals of each generation at a load is kept at 44, and the optimization is terminated at the $28^{th}$ generation, in which the optimized objectives and parameters are observed to converge to the Pareto front surface according to the convergence criteria described in Ref. [61].

# 3. Results and discussions

## 3.1. Correlation analysis of performance metrics and operating parameters

In order to identify the sensitive operating parameters and their coupling characteristics for the $DI^2$ strategy at different engine loads, the correlation analysis of performance metrics and operating parameters are performed for three typical operating loads, as shown in Fig. 4. Herein, the spearman correlation coefficient is selected to evaluate the degree and direction of the correlation between metrics and parameters based on all the cases computed in the optimization process, considering its superiority to deal with outlier and lower requirements of data distribution. From Fig. 4(a), it can be found that the fuel economy and emissions of the engine at low load are greatly affected by $p_{IVC}$, B-SOI, D-SOI, and D-$P_{Inj}$. For mid-load operation, the EGR rate, $R_b$, D-SOI, and $p_{IVC}$ are more crucial, and D-SOI shows a significantly positive correlation with $NO_x$ emissions (see Fig. 4(b)). For the high-load condition, the effects of EGR rate, $R_b$, and $p_{IVC}$ on performance metrics are highlighted. The crank angle of 10% heat release point (CA10) is an important indicator of the start of combustion in engines. Comparing the correlation coefficients between CA10 and operating parameters at different loads, it can be found that at low load, the ignition timing and subsequent initial heat release processes are basically governed by the initial intake pressure and the injection timings of diesel and n-butanol, and CA10 is negatively correlated with diesel injection timing and positively correlated with n-butanol injection timing. For the mid-load condition, the initiation of combustion is determined by diesel injection timing and EGR rate, and the influence of the n-butanol injection event can be ignored. However, different from the mid-load condition, the impact of n-butanol becomes prominent at high load, and its CA10 is closely relevant to the initial intake temperature, as well as the injection timing and injection pressure of n-butanol.

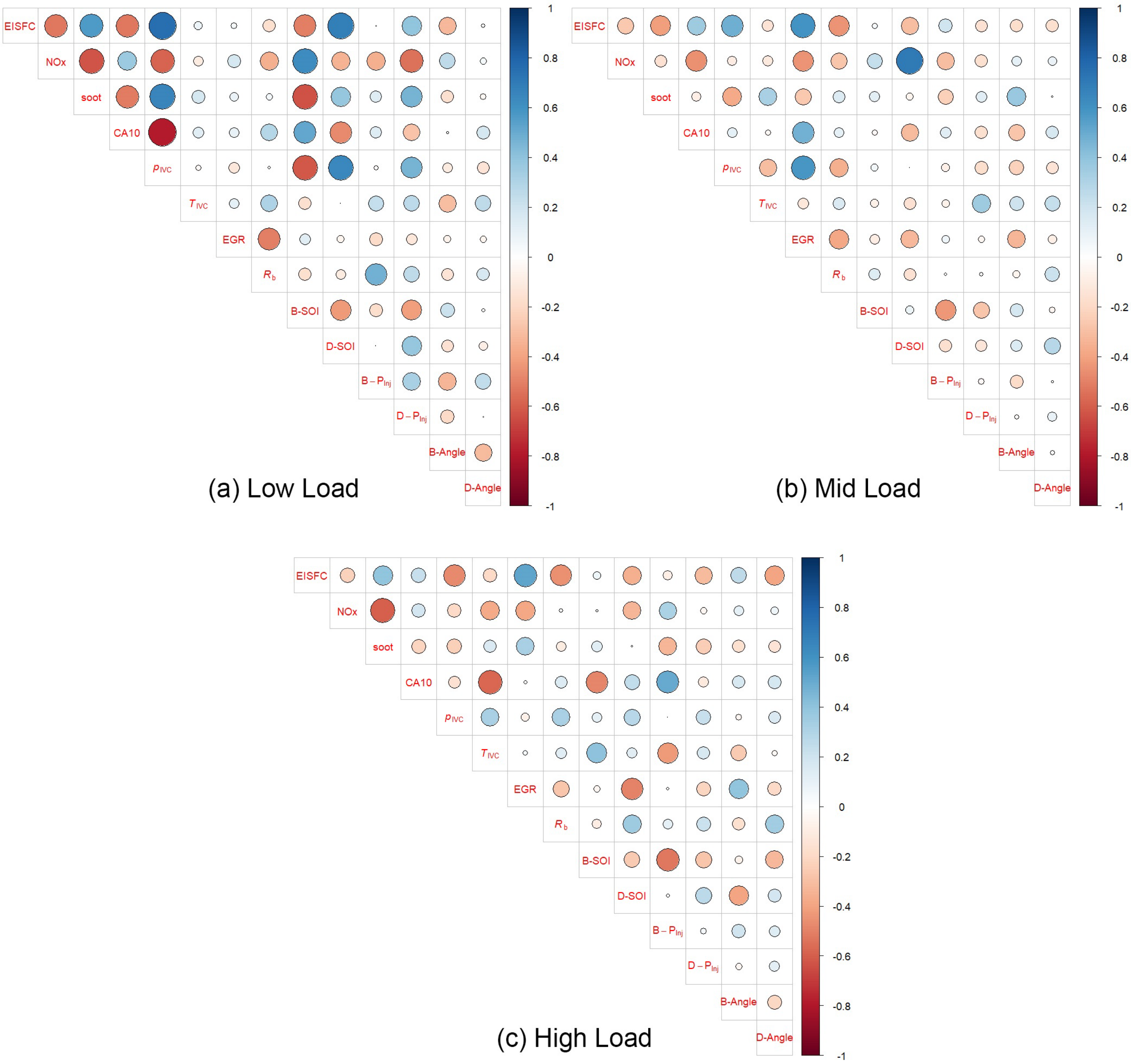


Fig. 4. Correlation analysis of operating parameters and performance metrics at low, mid, and high loads.

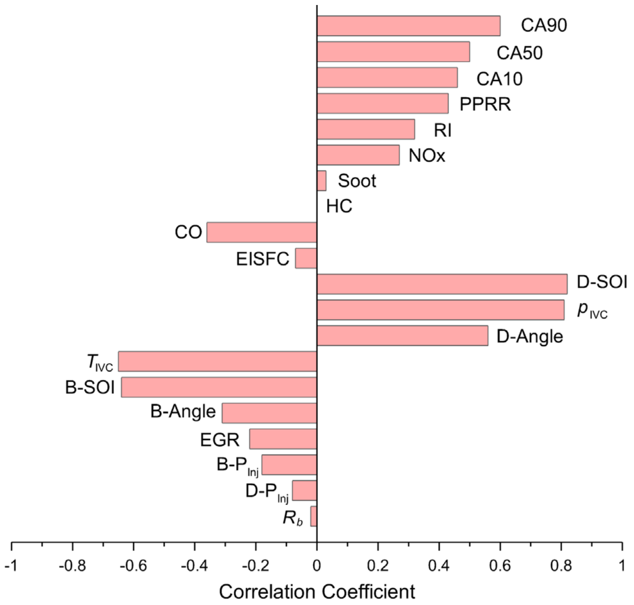


Fig. 5. Correlation analysis of load with operating parameters and performance metrics.

Fig. 5 shows the correlation analysis of performance metrics and full operating parameters with respect to engine load variation. The purpose is to explore the operating parameter selection and metric differences at different loads. Herein, the correlation coefficient is calculated utilizing all the cases involved in the three load optimizations of $DI^2$, where unreasonable and misfire cases are excluded, and the total fuel energy supplied per cycle is used to represent the change in the engine load level. It can be seen that EISFC, HC, and soot emissions keep very small variation in the full engine load range, while $NO_x$ and RI increase with load due to locally richer fuel/air mixture and more intensive in-cylinder combustion. Thus, in order to adapt to high-load operation, the combustion phasing of the engine (i.e., CA10, CA50, and CA90) needs to be delayed properly with increasing load. Notably, the CO emissions are reduced under high load conditions. Overall, to realize the application of the $DI^2$ strategy in the full load range, some operating parameters need to be modulated. As the load increases, the intake temperature ($T_{IVC}$) and pressure ($p_{IVC}$) should be decreased and increased accordingly. Moreover, as evident from Fig. 5, the injection timings of both n-butanol and diesel vary considerably with load levels. When the engine operation is converted from low to high loads, the n-butanol injection timing needs to be advanced while the diesel injection timing should be retarded, and a wider diesel spray angle is also needed.

## 3.2. Optimal fuel injection strategies and intake conditions of $DI^2$ at different loads

At different loads, the engine usually presents distinctive combustion features and limitations. At low load, because of the lower fueling quantity, as well as the lower in-cylinder temperature and pressure, insufficient combustion is the main constraint of engine operation, especially for the highly premixed low-temperature combustion strategies, such as HCCI and RCCI [7,62]. However, for high load, the enhanced thermal condition in the cylinder tends to cause premature ignition and high pressure rise rate. Fig. 6 illustrates the distributions of the final optimal intake conditions ($p_{IVC}$, $T_{IVC}$, and EGR rate) of $DI^2$ under different loads based on the statistical results of the Pareto front solutions. It is found that in order to avoid excessively diluted fuel/air mixture, the initial in-cylinder pressure of the engine at low load is concentrated in a low-pressure range of 1.0–1.2 bar, while at high load, the intake air needs to be enhanced to a high boost pressure level of 2.6–3.0 bar to ensure sufficient oxygen for the complete fuel oxidation. As the engine load increases, the mean value of the optimal initial in-cylinder temperature gradually decreases, varying from 385 K at low load to 363 K at high load, with the aim to alleviate low-load combustion efficiency and high-load pre-ignition problems, as shown in Fig. 6(b). Also, in order to avoid high $NO_x$ production in $DI^2$, a moderate EGR rate is needed in the full load range.

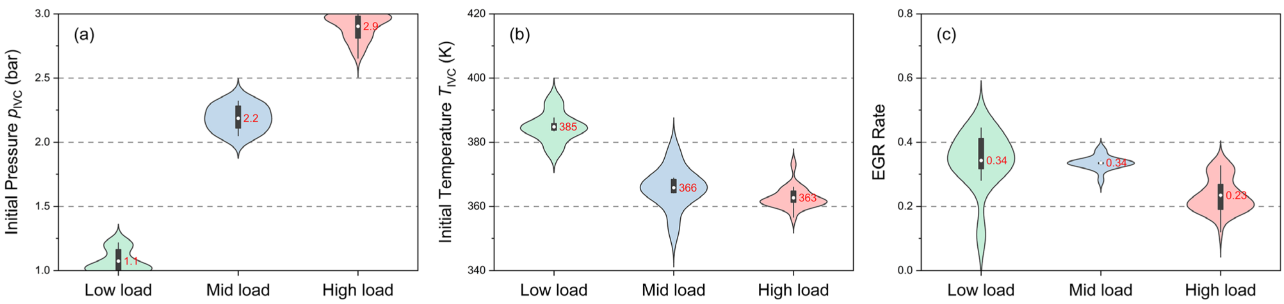


Fig. 6. Distributions of the final optimal intake parameters of $DI^2$ under different loads.

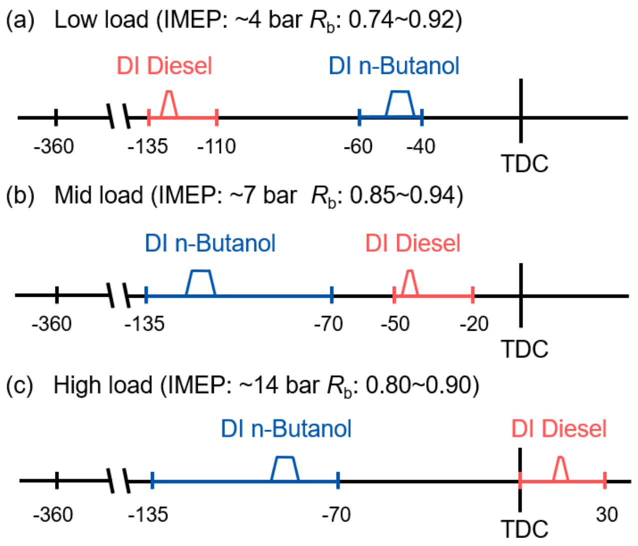


Fig. 7. Optimal fuel injection strategies of DI$^2$ at different engine loads.

Aiming at the respective operating characteristics of different engine loads, except for controlling intake boundary conditions, DI$^2$ also typically needs different fuel injection strategies and thereby different in-cylinder stratification charge. To some extent, the fuel injection strategy is more important for engine performance due to its close correlation with the in-cylinder dual fuel mixing process. The final optimal fuel injection strategies for DI$^2$ at low, mid, and high loads are summarized in Fig. 7. It is found that the high n-butanol energy ratio of 0.74 to 0.94 is adopted in the full load range. However, there exist significant differences in the dual fuel injection sequence and injection timing. For low-load conditions, a low-proportion diesel near 20% is first pre-injected into the cylinder around -135 to -110 °CA ATDC, while the optimal injection timing for the low-reactivity n-butanol is between -60 and -40 °CA ATDC. In fact, the low-load fuel strategy of DI$^2$ is similar to RCCI with reverse reactivity stratification (R-RCCI) [63] or dual-fuel sequential combustion (DFSC) [64] concepts, where the high-reactivity fuel is delivered into the cylinder by PFI and the low-reactivity fuel is directly injected into the cylinder well before or near the TDC. The main difference from R-RCCI and DFSC is that for the present low-load DI$^2$ strategy, the high-reactivity diesel is directly injected into the cylinder using an independent injector, thus the concentration stratification of diesel is introduced, and its degree and spatial distribution can also be adjusted by the dual fuel split ratio, as well as diesel injection timing and angle. In mid load, an opposite dual fuel injection sequence is adopted. Similar to the stratification concept of RCCI, the optimal mid-load $DI^2$ fuel strategy is to inject n-butanol into the combustion chamber early in the compression stroke to form a partially premixed n-butanol/air mixture, followed by a late diesel injection event at -50 to -20 °CA ATDC. As for the high-load $DI^2$ operation, n-butanol is still partially premixed in advance (-135~-70 °CA ATDC), while the diesel injection is delayed until after TDC. It is worth noting that for the $DI^2$ strategy, its dual fuel injection events are fully decoupled, so the above two types of fuel injection sequences can be implemented simultaneously under different loads in the same engine, which is not possible for dual fuel RCCI or DFSC engines that have a pre-fixed fuel sequence.

To analyze the heat release and stratified combustion characteristics of the optimal $DI^2$ strategies under different engine loads, three typical cases with the best fuel economy are respectively selected from the optimization results of the three loads as baseline cases, and their detailed information is listed in Table 2. Fig. 8 illustrates the variation of the in-cylinder pressure and heat release rate of the three typical cases. It can be observed that as the engine load increases, the combustion duration needs to be prolonged accordingly. For the high-load condition, its optimal combustion phasing is later and the combustion process behaves a two-stage heat release feature, corresponding to the sequential exotherm of n-butanol and diesel. In this combustion mode, the combustion events of n-butanol and diesel are separated. The n-butanol injected before -70 °CA ATDC is partially premixed and responsible for ignition and the first-stage combustion, while the diesel injected after TDC is ignited immediately after injection, resulting in the subsequent diffusion-controlled second-stage combustion. The late diesel injection helps to increase engine output power and IMEP, and reduce the fuel reactivity during the auto-ignition period to avoid premature combustion and high pressure rise rate at high load. Moreover, because the diesel is injected at the later stage of the n-butanol combustion, it can re-burn the unoxidized products from the n-butanol reaction to reduce HC and CO emissions, as shown in Table 2. According to Fig. 8, the in-cylinder pressure and heat release rate at low load are significantly lower, and both the heat release profiles for low and mid loads present a unimodal pattern, making it difficult to clarify the dual fuel combustion process just depending on the pressure and heat release histories. Considering the significant differences in the optimized dual fuel supply methods at low and mid loads, the effect of the fuel injection sequence on $DI^2$ combustion will be examined in the next section.

Table 2 Operating parameters and engine performance of the optimal $DI^2$ cases under different loads.

| Operating parameters | Low load | Mid load | High load |
|---|---|---|---|
| $p_{IVC}$ (bar) | 1.1 | 2.1 | 3.0 |
| $T_{IVC}$ (K) | 377.9 | 368.4 | 365.8 |
| EGR Rate | 0.34 | 0.34 | 0.19 |
| n-Butanol Energy Fraction, $R_b$ | 0.76 | 0.94 | 0.89 |
| n-Butanol SOI Timing, B-SOI (°CA ATDC) | -48.8 | -126.2 | -78.4 |
| Diesel SOI Timing, D-SOI (°CA ATDC) | -132.3 | -50.0 | 26.3 |
| n-Butanol Injection Pressure, B-$P_{Inj}$ (MPa) | 129.4 | 142.6 | 131.3 |
| Diesel Injection Pressure, B-$P_{Inj}$ (MPa) | 93.1 | 108.0 | 123.4 |
| n-Butanol Spray Angle, B-Angle (°) | 77.6 | 42.7 | 57.4 |
| Diesel Spray Angle, D-Angle (°) | 59.3 | 79.9 | 78.8 |
| **Engine performance** | **Low load** | **Mid load** | **High load** |
| EISFC(g/kWh) | 176.6 | 166.9 | 173.3 |
| $NO_x$ (g/kWh) | 0.052 | 0.00094 | 0.06 |
| Soot (g/kWh) | 0.00024 | 0.00052 | 0.00019 |
| HC (g/kWh) | 1.19 | 0.035 | 0.29 |
| CO (g/kWh) | 16.63 | 18.32 | 5.11 |
| RI ($MW/m^2$) | 2.23 | 2.69 | 4.03 |

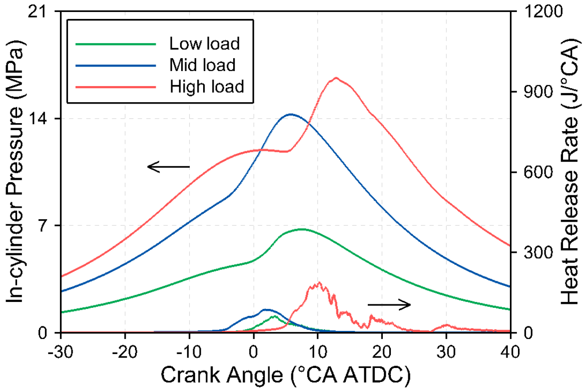


Fig. 8. Variation of the in-cylinder pressure and heat release rate of the three typical cases.

## 3.3. Effect of the injection sequence of n-butanol and diesel on DI$^2$ combustion

As indicated in Fig. 7, the optimal fuel strategy of DI$^2$ at low-load conditions is to inject the low-reactivity n-butanol into a high-reactivity diesel atmosphere, which is just opposite to its mid- and high-load situations. Therefore, to elucidate the reason for the difference in the optimal fuel supply strategies under different loads, as well as the effect of dual-fuel injection sequence on the in-cylinder combustion and emissions, based on the selected three typical cases, the injection timings of n-butanol and diesel at low and mid loads are exchanged for further comparison while the rest parameters remain the same as listed in Table 2. The cases with optimal and reverse dual-fuel injection sequence at low and mid loads are respectively denoted as D/B DI$^2_{Low}$, B/D DI$^2_{Low}$, D/B DI$^2_{Mid}$, and B/D DI$^2_{Mid}$, and their detailed engine performance is tabulated in Table 3. It is found that at low load, the D/B DI$^2_{Low}$ case shows a remarkable combustion efficiency advantage with respect to the B/D DI$^2_{Low}$ case. However, the D/B DI$^2_{Mid}$ case under the mid-load operating point exhibits significant deficiencies and tends to produce higher $NO_x$ emissions and combustion noise.

Table 3 Engine performance metrics of typical cases with optimal and reverse dual fuel injection sequences at low and mid loads.

| Engine performance | Low load | | Mid load | |
|---|---|---|---|---|
| | (a) D/B $DI^2_{Low}$ B-SOI=-48.8 °CA D-SOI=-132.3 °CA | (b) B/D $DI^2_{Low}$ B-SOI=-132.3 °CA D-SOI=-48.8 °CA | (c) B/D $DI^2_{Mid}$ B-SOI=-126.2 °CA D-SOI=-50.0 °CA | (d) D/B $DI^2_{Mid}$ B-SOI=-50.0 °CA D-SOI=-126.2 °CA |
| CA10 | -0.3 | -1.3 | -2.9 | 5.0 |
| CA50 | 3.7 | 1.7 | 2.0 | 8.3 |
| CA90 | 8.8 | 10.0 | 7.0 | 12.3 |
| Combustion Efficiency (%) | 97.4 | 75.2 | 97.5 | 93.0 |
| EISFC(g/kWh) | 176.6 | 232.2 | 166.9 | 189.1 |
| RI ($MW/m^2$) | 2.23 | 2.74 | 2.69 | 3.9 |
| $NO_x$ (g/kWh) | 0.052 | 0.023 | 0.00093 | 0.848 |
| Soot (g/kWh) | 0.00024 | 0.00062 | 0.00052 | 0.00012 |
| HC (g/kWh) | 1.19 | 57.35 | 0.039 | 5.48 |
| CO (g/kWh) | 16.63 | 54.10 | 18.23 | 38.41 |

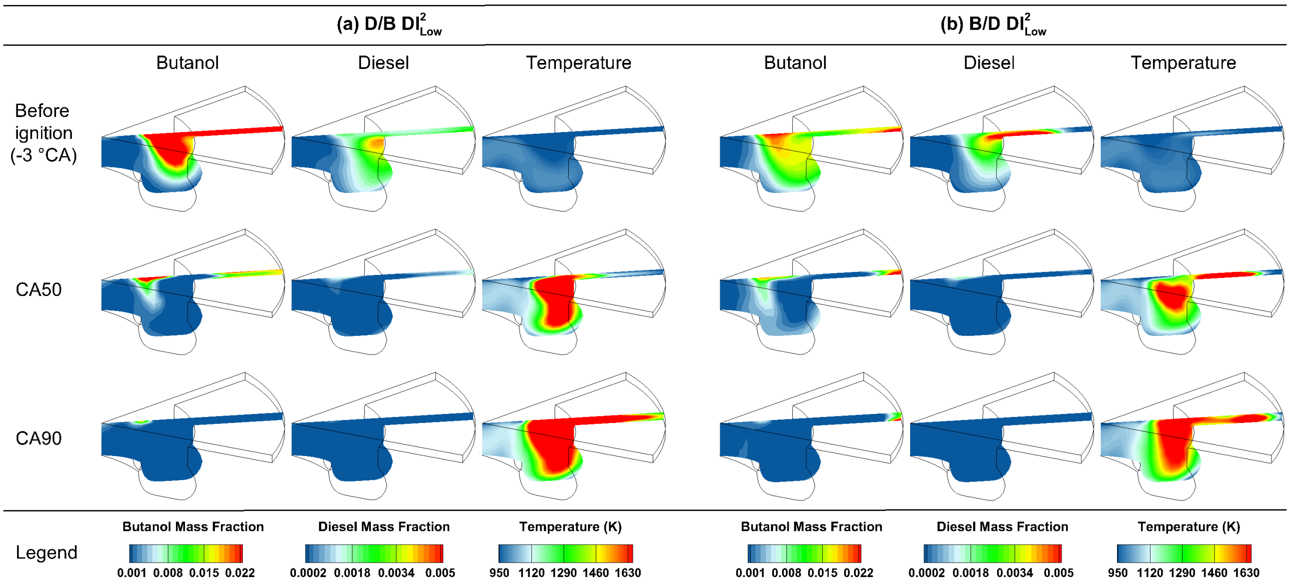


Fig. 9. Distributions of the in-cylinder temperature and the mass fraction of n-butanol and diesel at before-ignition, CA50, and CA90 for low-load cases with optimal and reverse dual-fuel injection sequences.

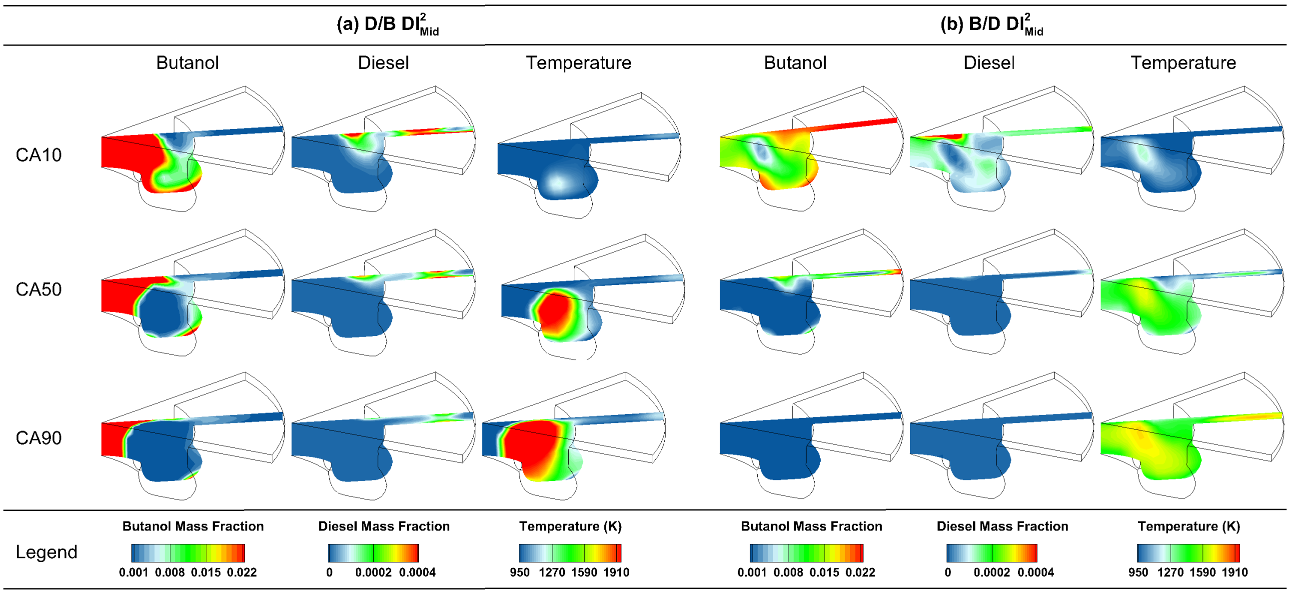


Fig. 10. Distributions of the in-cylinder temperature and the mass fraction of n-butanol and diesel at CA10, CA50, and CA90 for mid-load cases with optimal and reverse dual-fuel injection sequences.

Figs. 9 and 10 illustrate the distributions of the fuel concentration and temperature fields for low- and mid-load cases with optimal and reverse dual-fuel injection sequences, respectively. For low-load engine operation, it usually demonstrates lean in-cylinder fuel concentration and low global combustion pressure and temperature, and typically needs a relatively higher equivalence ratio to initiate the ignition and combustion processes. When adopting the injection strategy similar to mid and high loads where the n-butanol injection event is advanced to near IVC timing, it can be observed from Fig. 9 that compared with the case using late n-butanol injection (i.e., D/B $DI^2_{Low}$), the local fuel concentration of the pre-injected n-butanol in B/D $DI^2_{Low}$ before ignition is diluted more signifiicantly, and its distribution area is enlarged arising from the better evaporation characteristics and earlier injection timing than that of diesel. By this time, for the late injected diesel at -48.8 °CA ATDC, because of delayed injection timing and slower evaporation rate, the high-reactivity diesel vapor is mainly concentrated in a limited space at the edge of the piston bowl. Therefore, the local equivalence ratio and fuel reactivity near the combustion chamber axis and cylinder wall are quite low, which leads that the n-butanol distributed in these areas is only partially oxidized. As a result, as shown in Fig. 11, it can be found that at the end of combustion (i.e., 40 °CA ATDC), a large amount of HC and CO emissions are produced in the above areas for the B/D $DI^2_{Low}$ case.

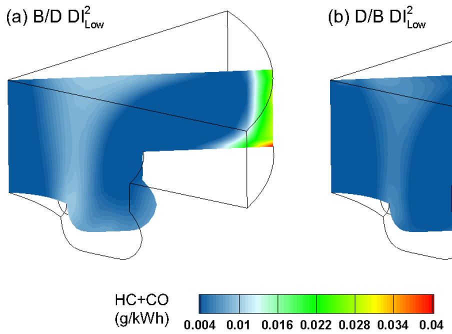


Fig. 11. Distributions of HC and CO emissions for low-load cases with optimal and reverse dual-fuel injection sequences at 40 °CA ATDC.

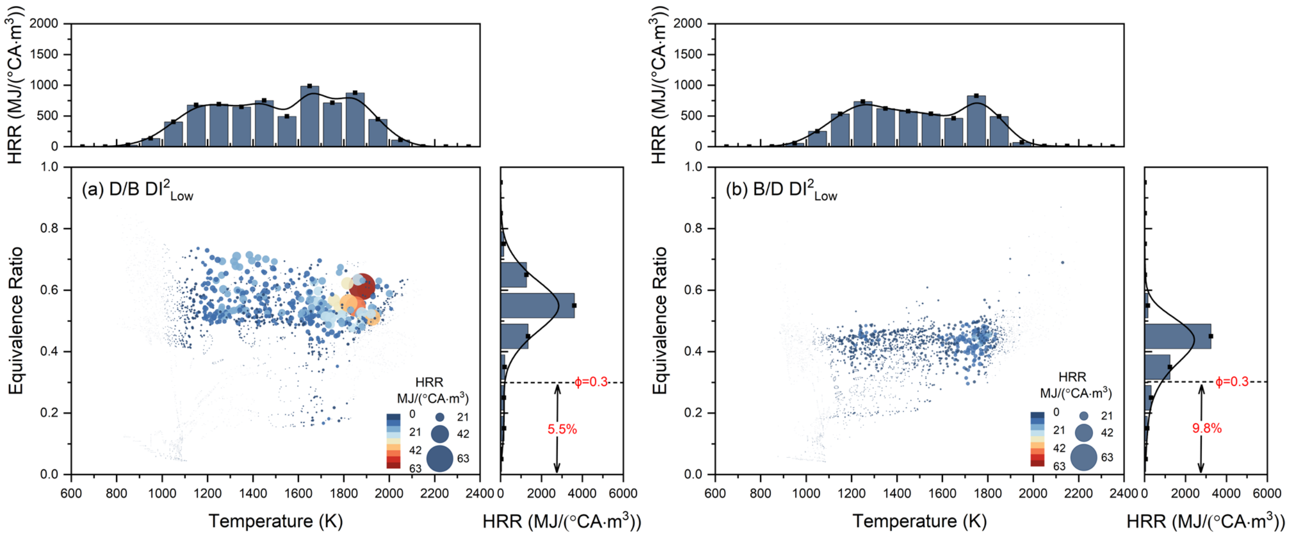


Fig. 12. HRR distributions in the temperature and equivalence ratio space for the low-load cases with optimal and reverse dual-fuel injection sequences at CA50.

Fig. 12 further depicts the distributions of HRR in the high temperature and equivalence ratio space for the D/B $DI^2_{Low}$ and B/D $DI^2_{Low}$ cases at 50% burning point (CA50). In this study, the calculation of equivalence ratio is based on the instantaneous atomic composition in a gas mixture following the work of Babajimopoulos et al. [65]. It is defined as the ratio of the number of oxygen atoms required for complete oxidation of H and C atoms in the mixture to the available oxygen atoms, and is expressed as follows:

$$\text{Equivalence ratio} = \frac{\sum_{i=1}^{N} 2\mathrm{C}_i[X_i]+0.5\mathrm{H}_i[X_i]}{\sum_{i=1}^{N} \mathrm{O}_i[X_i]} \tag{3}$$

where *N* is the total species number in the mixture, and $\mathrm{C}_i$, $\mathrm{H}_i$, and $\mathrm{O}_i$ correspond to the atomic number of carbon, hydrogen, and oxygen in $i^{th}$ species, respectively; $[X_i]$ is the molar concentration of the $i^{th}$ species. It can be found from Fig. 12 that the in-cylinder equivalence ratio of the low-load $DI^2$ operation is basically below 0.8 and exhibits a high proportion of heat release in the low-temperature interval less than 1600 K, especially for the n-butanol pre-injection situation. The statistical results of HRR indicate that for the D/B $DI^2_{Low}$ case, the major fuel exotherm is distributed in an equivalence ratio range of 0.5–0.6. However, for the B/D $DI^2_{Low}$ case, because of the better evaporation and mixing of the early injected n-butanol, its local equivalence ratio is migrated to a lower interval, and its main HRR is between 0.4 and 0.5. Moreover, compared with D/B $DI^2_{Low}$, more combustion of B/D $DI^2_{Low}$ occurs in the ultra-low equivalence ratio range of 0.0–0.3, accounting for 9.8% of the total heat release, approximately twice that of D/B $DI^2_{Low}$, which is potential to produce more HC and CO emissions.

Different from the low-load operation, the fuel loading and in-cylinder pressure are much higher at mid-load conditions, which makes the fuel/air mixture easier to ignite than that at low load under the same equivalence ratio. Therefore, although an advanced n-butanol injection timing of -126.2 °CA ATDC and a lower equivalence ratio than that of the low-load case (see Fig. 13(b)) are applied in the B/D $DI^2_{Mid}$ case, the in-cylinder distributed n-butanol can also be well oxidized at CA90, as shown in Fig. 10(b). Conversely, for the D/B $DI^2_{Mid}$ case where the start of injection timing of n-butanol is postponed to -50 °CA ATDC, the injected n-butanol is located in the piston bowl, and its local fuel concentration becomes fairly high due to the shortened mixing time. This results in more concentrated fuel heat release and higher combustion temperature that in turn intensify the formation of $NO_x$ emissions and increase combustion noise. The data obtained in Fig. 13 indicates that relative to B/D $DI^2_{Mid}$ the main HRR of D/B $DI^2_{Mid}$ indeed shifts to a higher equivalence ratio range of 0.6–0.8, and its HRR distribution is dispersed throughout the temperature and equivalence ratio space, yielding increased combustion inhomogeneities and decreased fuel economy. According to Fig. 13(a), in the D/B $DI^2_{Mid}$ case, there exist significant fuel exotherm in the high-temperature interval above 2000 K, where approximately 87.6% of total $NO_x$ mass is associated with the local fuel-rich and high-temperature region formed by the late injected n-butanol, as illustrated by Fig. 10(a). Therefore, to prevent the combustion limits from RI and $NO_x$, the fuel strategy to inject n-butanol into the diesel atmosphere is deprecated at mid-load conditions.

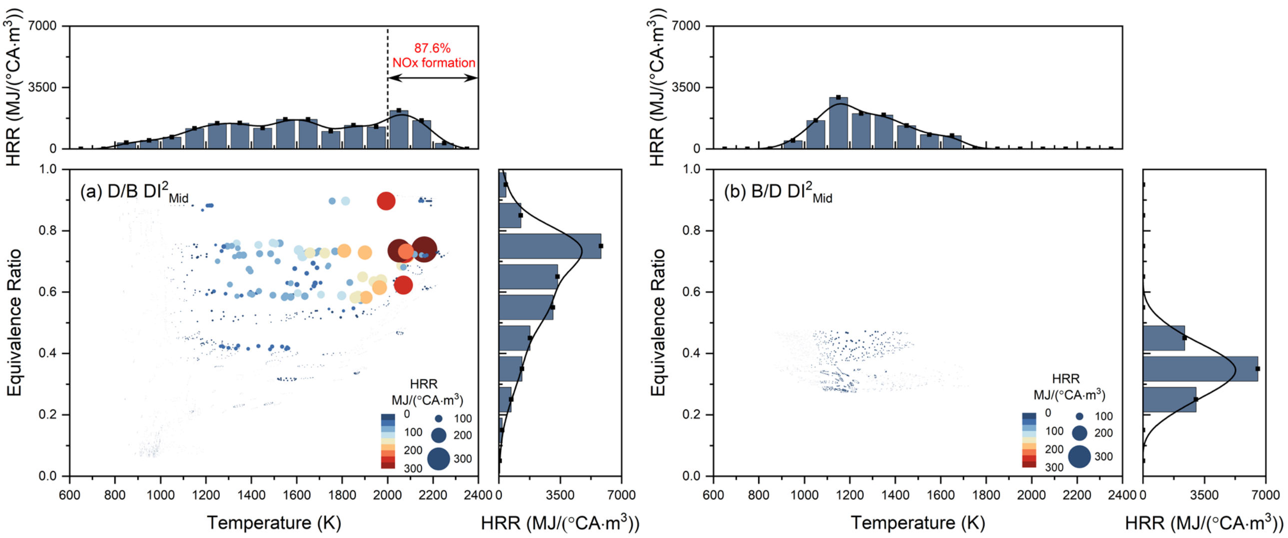


Fig. 13. HRR distributions in the temperature and equivalence ratio space for the mid-load cases with optimal and reverse dual-fuel injection sequences at CA50.

In summary, compared with pre-injected n-butanol, delaying n-butanol injection at low load is beneficial to enriching the concentration of the local fuel/air mixture in the cylinder to avoid excessively lean fuel/air mixture and further reduce the combustion occurring in the ultra-low equivalence ratio and temperature ranges, which is considered to be the main source of incomplete combustion at low load. Moreover, in D/B $DI^2_{Low}$, the diesel injected close to the IVC timing can be more evenly distributed in the cylinder, thus ensuring the fuel near the cylinder wall and combustion chamber center also has sufficient reactivity to be completely oxidized. In comparison, for mid-load conditions with increased fuel loading and combustion pressure, when retarding the n-butanol injection into the diesel atmosphere, it leads to a much higher local concentration of n-butanol and significant stratification in equivalence ratio and temperature, increasing combustion inhomogeneity of the premixed mixture, which deteriorates fuel economy and produces more intensive oxidation reactions and higher local combustion temperature, yielding significantly increased $NO_x$ emissions and high combustion noise. Thus, in the mid load, the optimal fueling strategy tends to inject n-butanol into the cylinder early in the compression stroke to form a partially premixed and homogeneous n-butanol-air mixture in advance and then followed by the diesel injection well before TDC. As for the high-load situation, its optimal fuel strategy is similar to that of mid load, except that the injection timing of diesel is retarded. Concerning the effects of fuel injection parameters of $DI^2$, it will be described in detail in the next section.

### 3.4. Effect of fuel injection parameters on $DI^2$ combustion and emissions at different loads

As mentioned above, focusing on the operating characteristics of various engine loads, $DI^2$ typically requires different charge preparation processes and therefore different fueling strategies. Considering the strong dependency of the in-cylinder fuel/air mixture formation on the fuel injection parameters in the dual-fuel direct injection system, based on the selected baseline cases at the three engine loads listed in Table 2, the effect of crucial fuel injection parameters on the combustion and emissions of n-butanol/diesel $DI^2$ is further analyzed in this section, including the injection timings of n-butanol and diesel and their spray angles.

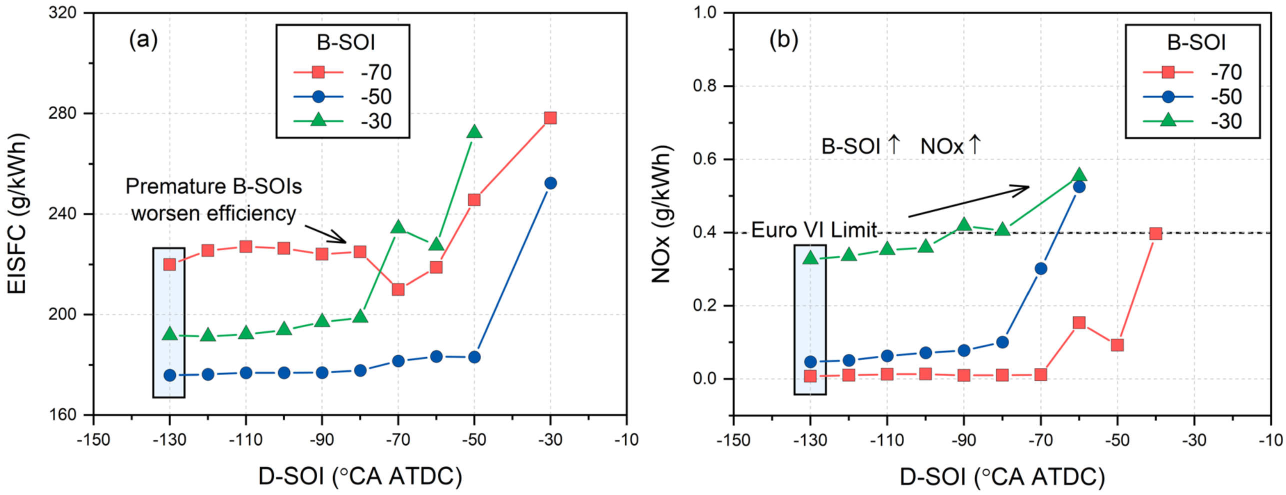


Fig. 14. Effects of B-SOI and D-SOI on EISFC and $NO_x$ emissions under $DI^2$ low-load conditions.

Fig. 14 illustrates the effect of B-SOI and D-SOI on EISFC and $NO_x$ emissions of $DI^2$ at low load conditions. It can be found that compared with diesel, the n-butanol injection event is more important to engine performance at low loads. The premature or too-late n-butanol injection can lead to deteriorated fuel efficiency, especially for the n-butanol injection earlier than -70 °CA ATDC. Moreover, consistent with the results from the low-load correlation analysis, $NO_x$ emissions and B-SOI at low load are positively correlated, as indicated in Fig. 14(b). A late B-SOI tends to sharply increase the formation of $NO_x$ emissions. Consequently, in order to keep a pleasant fuel economy and low $NO_x$ level, the optimal B-SOI is limited between -60 and -40 °CA ATDC. For the diesel injection event, it has little effect on engine performance when D-SOI is varied in the range of -130–-80 °CA ATDC, but further delaying its injection timing will cause significantly deteriorated EISFC and $NO_x$ owing to the worsened fuel/air mixing process.

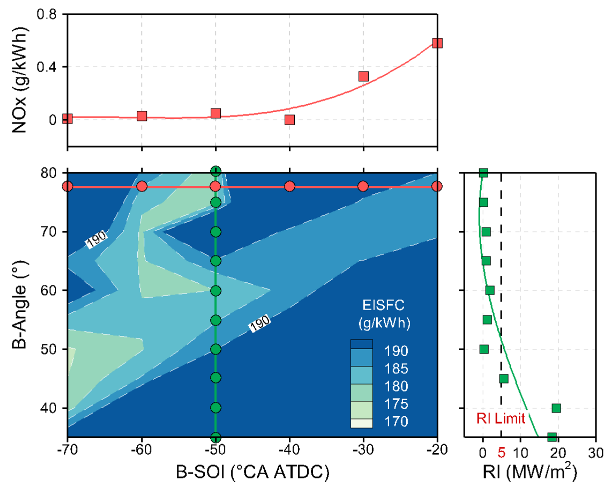


Fig. 15. Combined effect of B-SOI and D-SOI on engine performance under DI$^2$ low-load conditions.

At the optimal point of low load, diesel is injected into the cylinder at an early timing near IVC to form a highly premixed diesel/air mixture (see Fig. 9(a)), and then a high proportion of n-butanol is designed to introduce into this high-reactivity diesel atmosphere at a later injection timing. Therefore, compared with the well-mixed diesel, the injection timing and spray angle of n-butanol are more important in determining the mixing degree of the dual fuels and the in-cylinder stratification states. Therefore, it is necessary to further analyze the synergistic relationship between n-butanol injection timing and spray angle under low load. Fig. 15 shows the combined effect of B-SOI and B-Angle on engine performance. It is observed that the injection timing and spray angle of n-butanol exhibit a positive synergy. To maintain satisfactory fuel efficiency, when the injection timing of n-butanol is delayed, its spray angle also needs to increase accordingly. It is worth noting that when adopting a small n-butanol spray angle less than 50°, RI will increase dramatically. This is because a too small n-butanol spray angle distributes the fuel within the center of the combustion chamber, resulting in excessively concentrated heat release and high combustion noise.

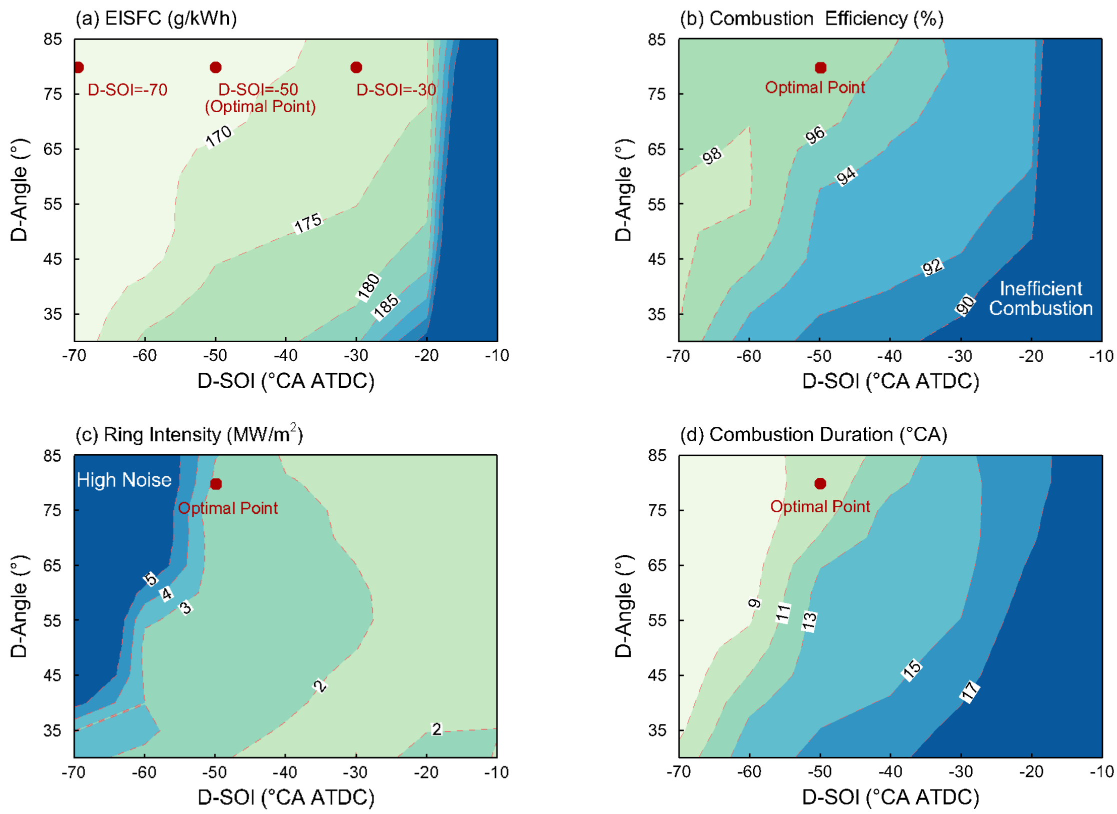


Fig. 16. Combined effect of D-SOI and D-Angle on engine performance under DI$^2$ mid-load conditions.

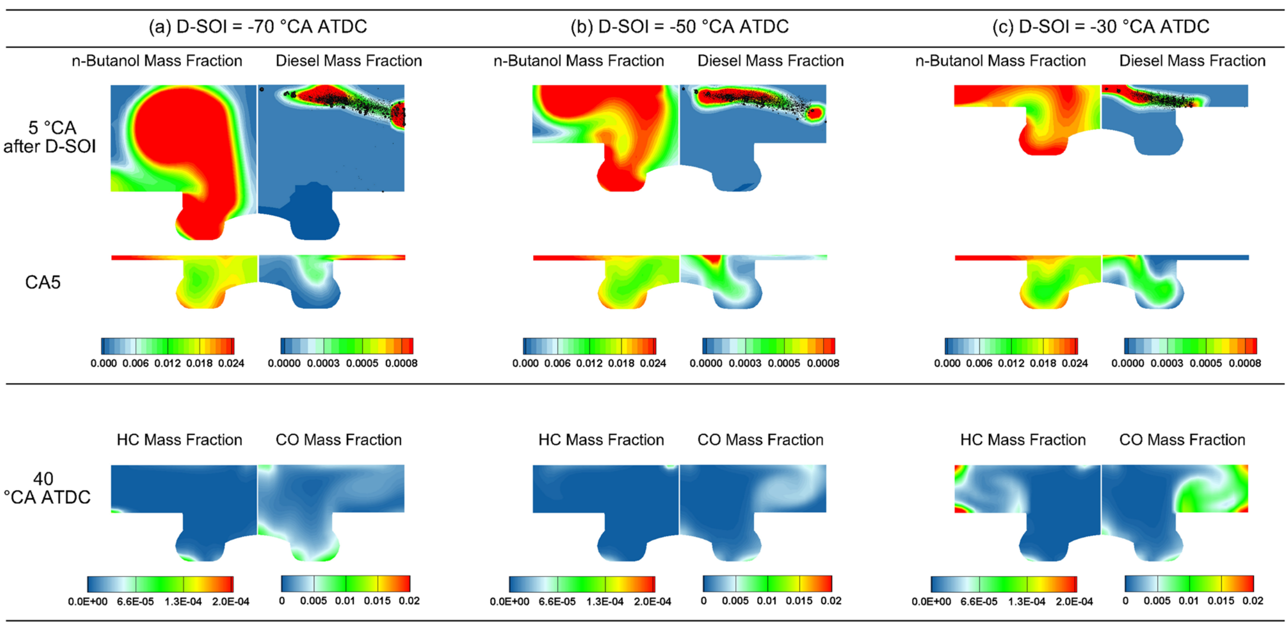


Fig. 17. Distributions of n-butanol (left cylinder) and diesel (right cylinder) at 5 °CA after D-SOI and CA5, as well as the sources of unburned HC and CO at 40 °CA ATDC, for the mid-load case with different D-SOI timings.

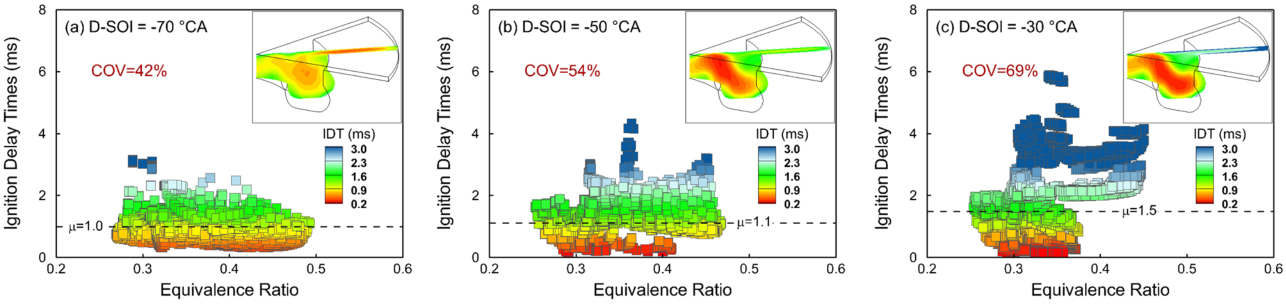


Fig. 18. Distributions of ignition delay times of the fuel-air mixture in the cylinder at CA5 for the optimal mid-load case with different D-SOI timings. (The plot is colored by the ignition delay time of the computational cells modelled as PSR reactors, and COV represents the dispersion degree of the ignition delay time distribution).

For mid-load conditions, the combined effect of D-SOI and D-Angle on $DI^2$ engine performance is shown in Fig. 16. It is found that when retarding diesel injection timing, the fuel economy is reduced due to the deteriorated combustion efficiency, while for the cases with D-SOI earlier than -50 °CA ATDC, high combustion noise is suffered, which is primarily correlated with the significantly shortened combustion duration, as shown in Fig. 16(d). To reveal the reasons for the changes in combustion efficiency and combustion duration, three D-SOI timings of -70, -50, and -30 °CA ATDC are selected for further analysis, as marked in Fig. 16(a). Fig. 17 depicts the spatial distributions of n-butanol and diesel at 5 °CA after diesel injection and 5% heat release point (CA5), as well as the main sources of unburned HC and CO at 40 °CA ATDC, for the mid-load case with different D-SOI timings. It is found that as D-SOI is delayed, the high-concentration area of diesel gradually shifts from the squish region to the center of the combustion chamber and becomes more concentrated. Specially, for the case with D-SOI of -30 °CA ATDC, the diesel is basically all distributed in the piston bowl, yielding that a large amount of n-butanol located in the low-temperature squish region cannot be fully oxidized due to the low local fuel reactivity, and therefore causing a lower combustion efficiency at a later D-SOI. Fig. 18 illustrates the distributions of ignition delay times (IDT) of the fuel-air mixture in the cylinder at CA5 for the different D-SOI cases. By modelling each computational cell in the simulation as a homogeneous reactor, the ignition delay time of each cell can be obtained based on the transient in-cylinder thermodynamic state and gas composition. The ignition delay time in the present study is defined as the time that the reactor temperature under the unreactive state is above its initial temperature of 400 K. In order to quantitatively describe the dispersion degree of the ignition delay time distribution in the cylinder at different D-SOIs, the coefficient of variation (COV) is introduced here and is expressed as

$$\mathrm{COV} = \frac{\sigma}{\mu} \tag{4}$$

where $\sigma$ and $\mu$ are the standard deviation and mean value of the ignition delay time of the in-cylinder computational cells.

It can be observed that under mid load, the in-cylinder ignition delay time is relatively insensitive to the local equivalence ratio of the mixture. When adopting a later diesel injection, the fuel reactivity stratification in the cylinder is enhanced and the region with short ignition delay time is more concentrated due to the shortened mixing time and more concentrated diesel distribution. Consequently, as shown in Fig. 18, for a later D-SOI timing, the ignition delay time of the in-cylinder local fuel/air mixture varies in a wider range, and the dispersion degree of ignition delay time increases, as indicated by the calculated COV value that increases from 42% at D-SOI of -70 °CA to 69% at D-SOI of -30 °CA, which tends to produce more obvious staged heat release and lower combustion rate, and ultimately longer combustion duration and lower engine noise. Therefore, in order to meet the RI limit and achieve a high combustion efficiency, the optimized diesel injection timing in the mid-load DI$^2$ strategy is limited between -50 and -20 °CA ATDC. As for the diesel spray angle, it has little effect on RI. However, a larger diesel angle helps to increase the chemical reactivity of the local fuel/air mixture in the squish region, which enhances the complete oxidation and therefore obtains a higher combustion efficiency at mid load. Note that as for the influence of n-butanol-relevant parameters under mid load, it has been discussed in detail in the authors' previous paper [27].

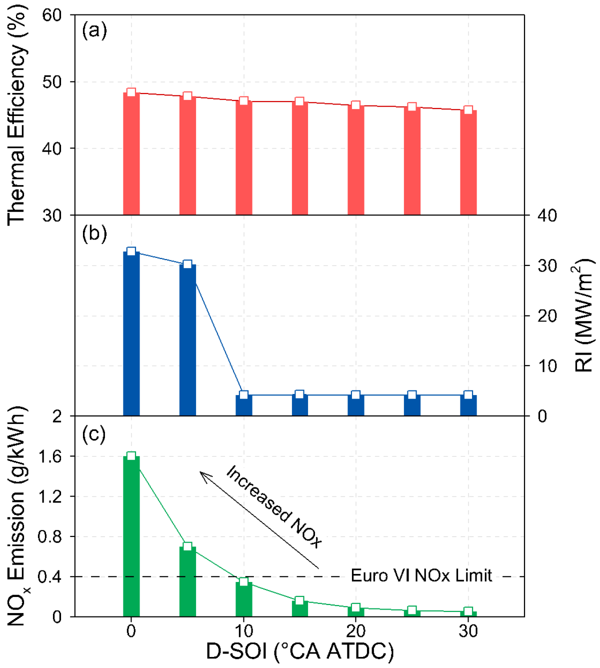


Fig. 19. Influence of D-SOI on the combustion and emissions of DI$^2$ under high load conditions.

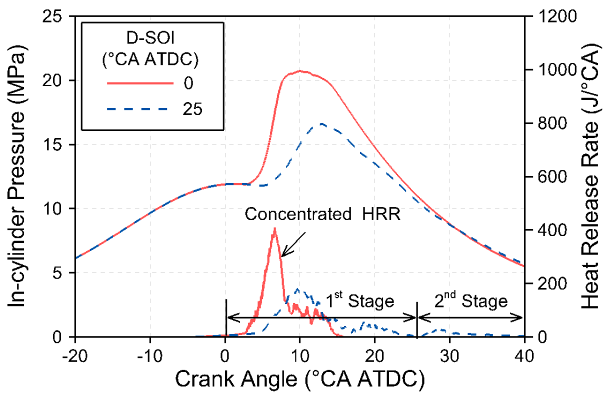


Fig. 20. In-cylinder pressure and HRR for the two cases with the D-SOI timings of 0 and 25 °CA ATDC.

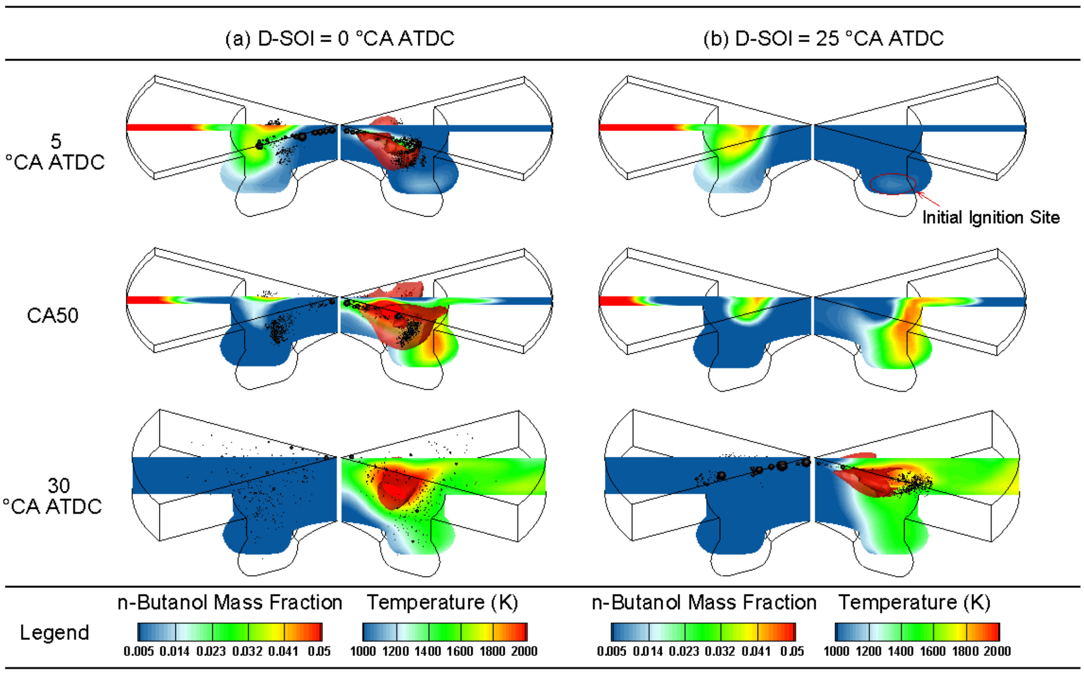


Fig. 21. In-cylinder n-butanol concentration and temperature distributions for the two cases with the D-SOI timings of 0 and 25 °CA ATDC. (Iso-surface in the plot corresponds to the region with the temperature of 2000 K)

In order to adapt high-load operation, a two-stage heat release process is used in the n-butanol/diesel DI$^2$ combustion. Similar to the optimal mid-load strategy, the n-butanol is still partially premixed in advance at high load, however, its diesel injection event is delayed after TDC. Thus, the influence of D-SOI on the combustion and emissions of DI$^2$ under high load conditions is examined, as illustrated in Fig. 19. For an earlier D-SOI, it can be seen from Fig. 19(a) that the thermal efficiency is slightly improved because of the lower exhaust and combustion losses. However, earlier D-SOI timing leads to a sharp increase in engine-out $NO_x$ emissions. When the D-SOI timing is earlier than 5 °CA ATDC, high combustion noise is also observed. Fig. 20 shows the in-cylinder pressure and heat release rate for the two cases with the D-SOI timings of 0 and 25 °CA ATDC. Compared with D-SOI of 25 °CA, the whole combustion process is advanced for D-SOI of 0 °CA ATDC, and shorter combustion duration and more concentrated HRR are observed. The in-cylinder temperature and n-butanol concentration distributions at the two D-SOI timings are shown in Fig. 21. It can be found that owing to the increased in-cylinder combustion pressure, temperature, and fuel mass under high load conditions, the high-reactivity diesel for D-SOI of 0 °CA ATDC is ignited quickly when being introduced into the cylinder, forming a diffusion-controlled high-temperature flame with the surrounding partially premixed n-butanol, which yields aggravated $NO_x$ production. Moreover, due to the ignition effect of diesel and the compression ignition of the n-butanol distributed at the bottom of the piston bowl, the fuel heat release is concentrated, tending to cause high pressure rise rate and engine noise.

Nevertheless, for the D-SOI of 25 °CA ATDC, the whole HRR is relieved and can be divided into two stages. The first-stage combustion corresponds to the low-temperature combustion of the partially premixed n-butanol and accounts for the major part of the total fuel heat release, while the second-stage heat release is mainly from the diffusion combustion of the post-injected diesel. Because the main combustion heat is from the n-butanol low-temperature combustion, the concentrated and intensive high-temperature combustion process encountered at early D-SOI timing can be effectively avoided. In addition, the diesel injected during the expansion stroke also contributes to improving IMEP without causing serious engine knock. For the diesel combustion at the second stage, due to the lack of the effect of n-butanol oxidation, its combustion temperature and intensity are also weaker relative to that with the D-SOI of 0 °CA ATDC. Therefore, under high load, the two-stage combustion strategy generated by later D-SOI is preferred, which helps to smooth heat release and achieve lower pressure rise rate and $NO_x$ emissions while maintaining engine output power.

## 3.5. Ignition mechanism analysis of the $DI^2$ strategy at different loads

For multi-load $DI^2$ combustion, the major challenge is to reasonably organize the dual fuel mixing process and the in-cylinder stratification to control fuel ignition and heat release profile for meeting the combustion requirements and limits at various loads. Thus, it is necessary to analyze the in-cylinder fuel stratification conditions and identify the key factors driving ignition under different loads. Fig. 22 illustrates the in-cylinder stratifications of temperature, equivalence ratio, and fuel reactivity for the optimal n-butanol/diesel $DI^2$ strategy under low, mid, and high load points before auto-ignition (i.e., -16 °CA ATDC). The spheres shown in the plot are colored by the ignition delay time of the computational cells in the CFD simulation. The fuel reactivity is represented by the cetane number (CN) and is computed based on the relative mole ratio of n-butanol and diesel in the mixture as Eq. (5):

$$CN_m = CN_b \cdot x_b + CN_d \cdot x_d \tag{5}$$

where $CN_m$, $CN_b$, and $CN_d$ are the cetane number of the mixture, n-butanol, and diesel, respectively; $x_b$ and $x_d$ represent the relative mole fractions of n-butanol and diesel. In the high-load condition, diesel is introduced into the cylinder at 26 °CA after TDC, and the first ignition of the fuel/air mixture only depends on the partially premixed n-butanol injected during the intake stroke. As shown in Fig. 22(c), the fuel reactivity in the cylinder nearly remains constant before the combustion initiation, but the equivalence ratio and temperature stratifications are much more obvious. The in-cylinder equivalence ratio distributes in a wide range of 0.0–1.0, and the temperature in the higher equivalence ratio region is lower due to the evaporation cooling of the directly injected n-butanol. The ignition delay time calculated from the in-cylinder computational cells shows that the region with high probability of ignition tends to be in the high-temperature space, especially in the equivalence ratio interval of 0.2 to 0.4. For the region with an equivalence ratio below 0.2, the ultra-lean fuel/air mixture makes it difficult to be ignited, yielding the longest ignition times. Overall, the fuel ignition is primarily controlled by the in-cylinder temperature distribution.

While for the mid-load situation, the equivalence ratio-temperature map shown in Fig. 22(b) indicates that the in-cylinder local equivalence ratio and temperature concentrate in the range of 0.2–0.6 and 750–850 K, respectively. Also, different from the low-level stratification in fuel concentration and temperature, the stratification of fuel reactivity is more obvious at mid load. This is mainly because the early injection of a high proportion of n-butanol (above 85% of the total fuel energy) at mid load can ensure the sufficient mixing of n-butanol and air, and therefore improve the uniformity of the in-cylinder charge and the temperature distributions before auto-ignition. In comparison, the late injection of a small amount of the high-reactivity diesel can increase the local diesel blending ratio to enhance the stratification in the fuel reactivity of the mixture. It can be found from the distribution of ignition delay time shown in Fig. 22(b) that the initial ignition sites tend to occur in the high fuel reactivity region that is related to the diesel directly injected at -50°CA ATDC, similar to the RCCI combustion. The enhanced local fuel reactivity in the cylinder acts as an initiator of ignition.

For the low load, it can be found from Fig. 22(a) that the fuel reactivity distributes in a much wider range, and the late n-butanol injection is beneficial to increasing the in-cylinder equivalence ratio so that the overly lean fuel/air mixture can be avoided. The region with a high probability of ignition under low load is more likely to be in the equivalent ratio range of 0.4 to 0.8 with moderate fuel reactivity and temperature.

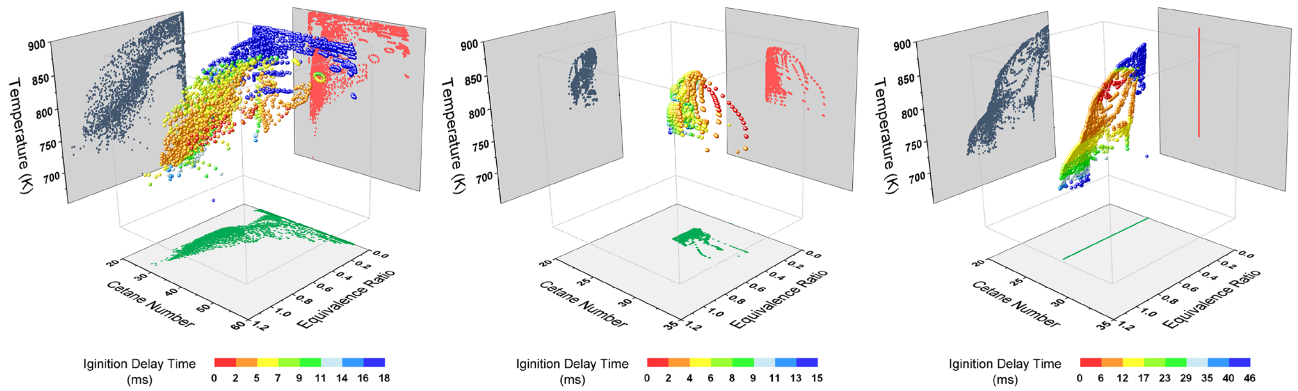

(a) Low Load (b) Mid Load (c) High Load

Fig. 22. Stratifications in the temperature, equivalence ratio, and fuel reactivity space for the n-butanol/diesel DI$^2$ strategy under low, mid, and high loads before auto-ignition (i.e., -16 °CA ATDC).

In order to further reveal the role of n-butanol and diesel in the DI$^2$ ignition process at low load, the ignition mechanism of the DI$^2$ strategy is analyzed in detail. Fig. 23 shows the distributions of mass fraction and destruction rate of diesel and n-butanol, in-cylinder temperature, and heat release rate at -16 °CA ATDC. At that time, the fuel is in the initial reaction stage and the in-cylinder temperature is in the range of 600–850 K. Due to the high latent heat of vaporization of the directly injected fuel and the slower temperature increase rate caused by the increased local heat capacity of the mixture, the temperature in the main concentration distribution region of n-butanol and diesel is significantly lower, especially for the high-proportion n-butanol distributed locations, as shown in Fig. 23(c). It can be seen that by this time the consumption of diesel and n-butanol and fuel heat release are mainly concentrated in the periphery of the high fuel concentration regions that has a relatively higher local temperature. This suggests that with respect to fuel concentration and reactivity, the temperature is a more crucial factor to determine where the initial fuel reaction occurs at low load. Moreover, comparing Figs. 23(d) and 23(e) shows that although n-butanol has a higher energy fraction relative to diesel at low load, the destruction rate of diesel is roughly 10 times that of n-butanol at this stage, indicating its higher reaction priority.

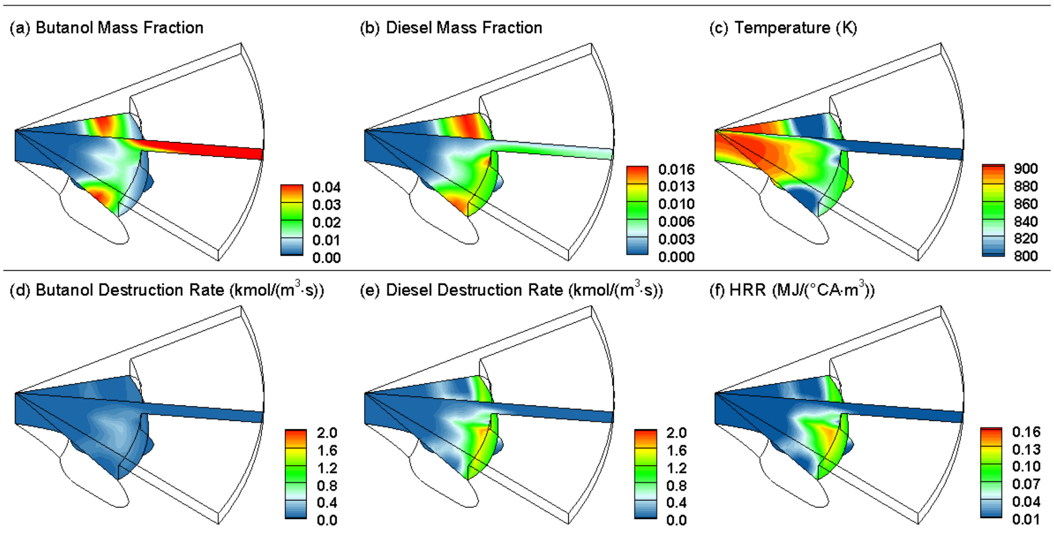


Fig. 23. Distributions of the mass fraction and destruction rate of n-butanol and diesel, in-cylinder temperature, and HRR of low-load $DI^2$ at -16 °CA ATDC.

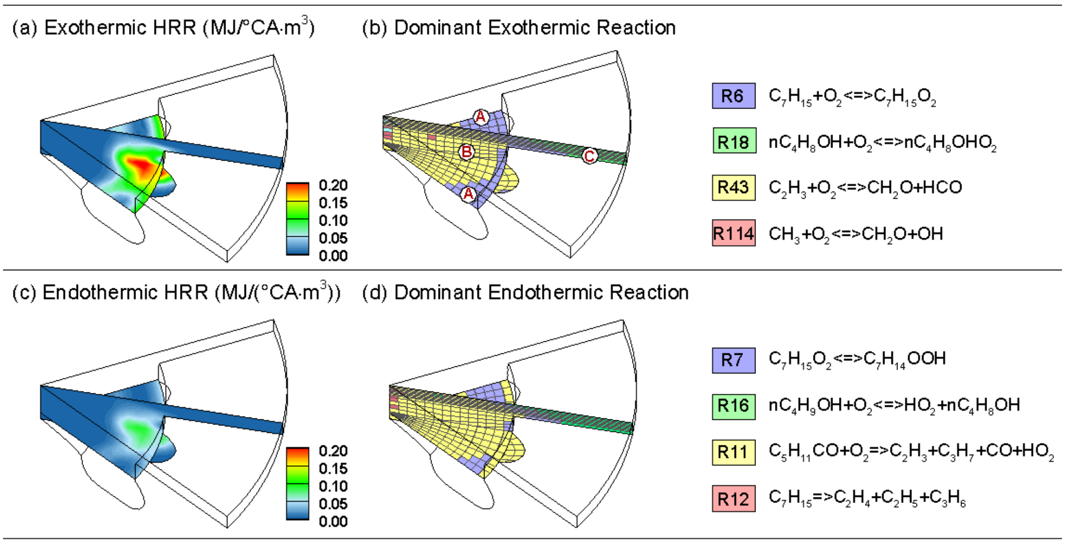


Fig. 24. Dominant reactions of the in-cylinder main reaction space of the low-load $DI^2$ strategy at -16 °CA ATDC.

Compared with mid- and high-load conditions, the ignition process of $DI^2$ at low load presents more complex features. Thus, in this paper, based on the reaction path analysis, the important fuel consumption and reaction paths that control the fuel ignition of $DI^2$ at low load are further identified. The dominant exothermic and endothermic reactions of the low-load $DI^2$ in the different combustion zones at -16 °CA ATDC are identified in Fig. 24. It is found that the main heat-releasing and heat-absorbing areas are located in the high-temperature region around the piston edge. The main reactions governing the in-cylinder heat production are R6 and R43, respectively. In the position A marked in Fig. 24(b), where a large amount of fuel is distributed, due to the lower local temperature (see Fig. 23(c)), the primary $O_2$-addition reaction of n-heptyl is mainly carried out. While for the high-temperature region B, the reaction process is accelerated, and the fuel release energy is mainly derived from the oxidation reaction R43 of the small hydrocarbon molecule $C_2H_3$ formed by n-heptane decomposition. For the liner region C, although the concentrations of n-butanol and diesel are high, the fuel destruction rate in this zone is slow due to the significantly low temperature, and currently its representative exothermic reaction is R18. Considering the heat absorbing process, the fuel-released energy of region B partially provides the decomposition of hydroperoxide ketone $C_5H_{11}CO$, which produces various active species, such as $C_2H_3$ and $HO_2$, and then supports the subsequent chain branching reactions and heat accumulation in this region. In the location A, the fuel-released heat is mainly used for the isomerization of $C_7H_{15}O_2$, while in the lowest temperature area C, the reaction process is the slowest and the first $O_2$-addition of n-butanol is still ongoing, and this reaction is a strong endothermic process and has a limited contribution to the alkyl accumulation.

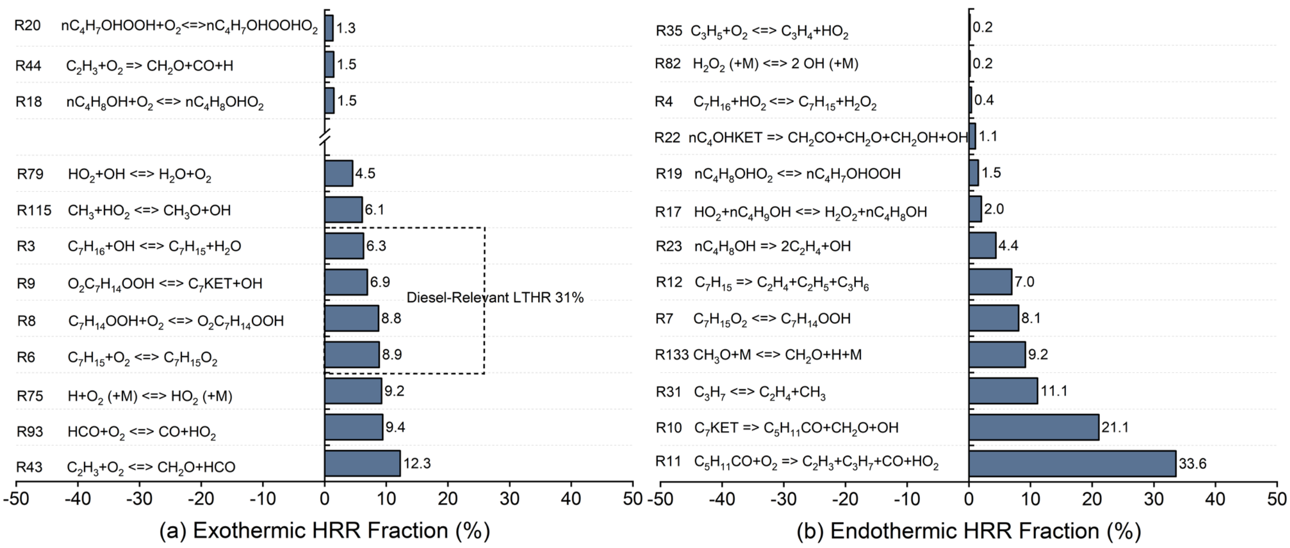


Fig. 25. Heat release statistics for the exothermic and endothermic processes of the low-load $DI^2$ strategy at -16 °CA ATDC.

Fig. 25 illustrates the main reactions that control the exothermic and endothermic processes of low-load $DI^2$ combustion at -16 °CA ATDC. As demonstrated in Fig. 25(a) for the exothermic HRR data, the fuel-released energy is primarily from the diesel low-temperature oxidation paths, particularly R6, R8, R9, and R3, involving the $O_2$-addition reactions of heptyl radical ($C_7H_{15}$) and heptyl peroxy radical ($C_7H_{14}OOH$), decomposition reaction of hydroperoxide radical ($O_2C_7H_{14}OOH$) to keto-peroxide $C_7KET$ and OH radical, and H-abstraction reaction of n-heptane through OH radical. The low-temperature heat release (LTHR) from n-heptane and its secondary oxidation products accounts for about 31% of heat production, while n-butanol solely takes about 4% partially listed in Fig.

25(a). From the endothermic HRR illustrated in Fig. 25(b), the main endothermic reactions include the decomposition of the low-temperature oxidation products $C_5H_{11}CO$, $C_7KET$, and $C_3H_7$ of n-heptane, which occupy approximately 54.7% of the total heat absorption and support the accumulations of the OH and $HO_2$ radicals to trigger the subsequent chain branching reactions.

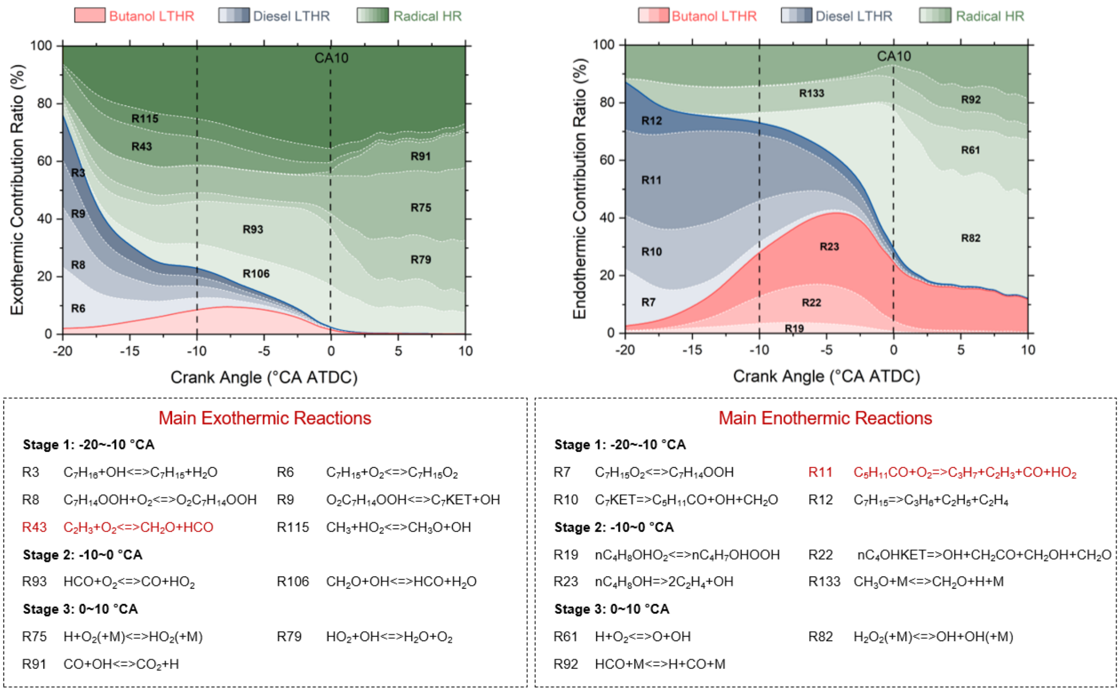


Fig. 26. Main reaction path analysis of the n-butanol/diesel DI$^2$ strategy at low load in the whole heat release process.

Fig. 26 shows the main reaction paths of the n-butanol/diesel DI$^2$ strategy at low load in the whole heat release process. It is observed that the entire reaction process can be divided into three combustion stages, i.e., diesel-controlled low-temperature heat release (LTHR) stage (-20~-10 °CA), n-butanol decomposition stage (-10~0 °CA), and high-temperature oxidation stage (after 0 °CA). In the first stage, the LTHR of n-heptane and its low-temperature products occupies a fairly high proportion of the total released energy, and the endothermic process demonstrates that the absorbed heat is primarily used to support the n-heptane-relevant species decomposition and oxidation, which helps accumulate the initial radical pool, including reactions R7, R10, R11, and R12, while the LTHR from n-butanol has a negligible contribution to the heat and radical accumulation and temperature promotion at this stage. For the second stage, the heat generated by n-heptane and n-butanol LTHR is low, and the thermal energy is mainly from the oxidation of fuel intermediates. Meanwhile, it can be noticed that the consumption of n-butanol is highlighted, and the endothermic proportion of n-butanol-related decomposition reactions increases significantly, especially for R23 ($nC_4H_8OH$=>$2C_2H_4$+OH) and R22 ($nC_4OHKET$=>OH+$CH_2CO$+$CH_2OH$+$CH_2O$). In the third stage (i.e., after CA10), the in-cylinder thermal and active atmosphere are enhanced, and the combustion is shifted into the high-temperature oxidation stage. The dominant endothermic reactions mainly include the dissociation of hydrogen peroxide ($H_2O_2$) and the β-cleavage reaction of H and $O_2$, which are considered to be the indicator of ignition and high-temperature oxidation. The major reactions controlling the exothermic process are R75 (H+$O_2$(+M)<=>$HO_2$(+M), R79 ($HO_2$+OH<=>$H_2O$+$O_2$), and R91 (CO+OH<=>$CO_2$+H). Therefore, it can be concluded that in the optimal $DI^2$ strategy at low load, the pre-injected low-proportion diesel first participates in the reaction and releases substantial heat through the low-temperature oxidation paths to increase the system temperature and accumulate initial active radicals, which supports the subsequent decomposition and oxidation of the surrounding n-butanol, and therefore control ignition and combustion phasing.

Fig. 27 depicts the effect of the pre-injected diesel energy fraction on combustion phasing, thermal efficiency, and RI under the low-load fuel injection strategy for $DI^2$. It can be seen that the effect of the pre-injected diesel on the in-cylinder thermal condition and the active atmosphere is important during the initial ignition stage. By adjusting the diesel proportion a rapid and stable response of the ignition timing can be realized. When increasing the quantity of the pre-injected diesel, the entire combustion process can be significantly advanced. However, it is worth noting that when the diesel ratio is higher than 0.6, the ignition timing is too advanced near -6.6 °CA ATDC, which makes RI exceed the stable operation limit of 5 $MW/m^2$ and obviously deteriorates fuel efficiency. In addition, as can be seen from Fig. 27(a), when just using the neat n-butanol injection, misfire occurs, suggesting that the pre-injected diesel is essential to stabilize the n-butanol ignition under low load.

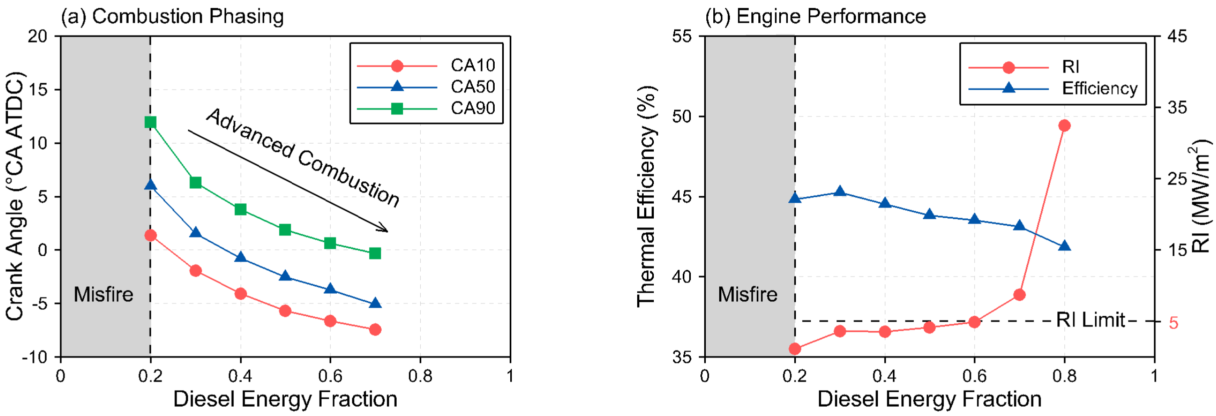


Fig. 27. Effect of the pre-injected diesel energy fraction on combustion phasing, thermal efficiency, and RI of the low-load DI$^2$ strategy.

# 4. Conclusions

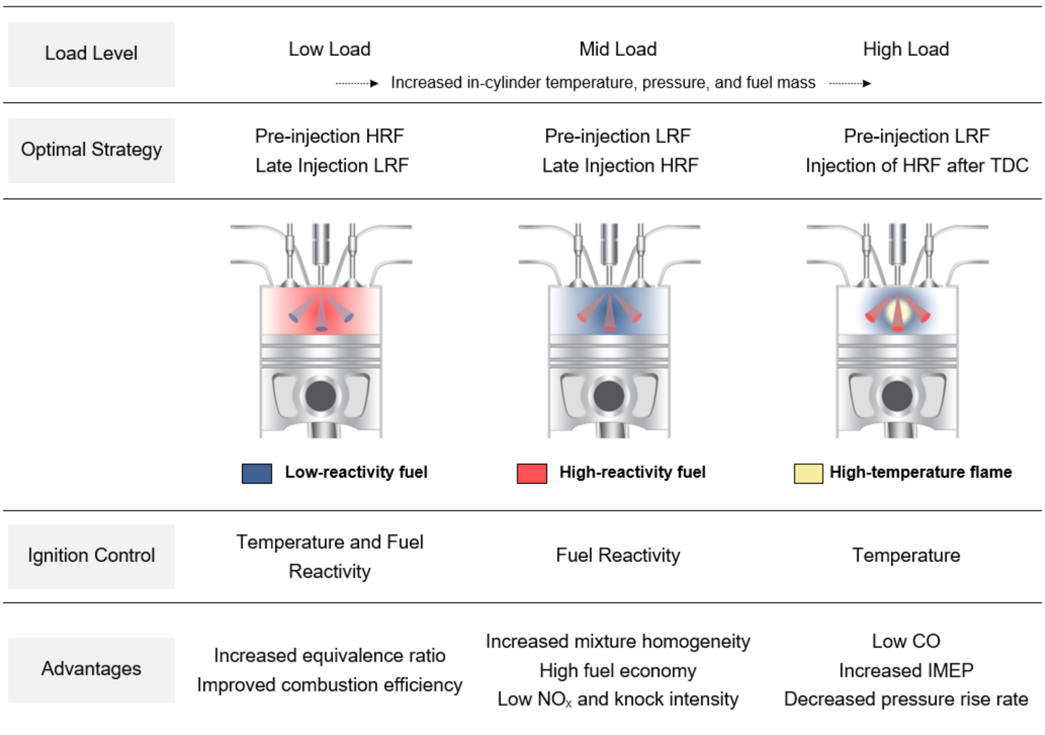


Fig. 28. Comparison of the optimal fuel strategy of DI$^2$ under different engine loads.

The optimal combustion modes of the n-butanol/diesel dual direct injection ($DI^2$) strategy under different engine loads obtained in the present investigation through numerical optimization are summarized in Fig. 28. The effects of the dual fuel injection sequence and crucial fuel injection parameters on the combustion and emissions of the $DI^2$ engine are examined. Moreover, the in-cylinder stratification characteristics and main factors driving the ignition for the optimal solutions at the three loads are further analyzed, and the key findings are summarized as follows:

(1) Under low-load conditions, the optimal $DI^2$ fueling strategy needs to pre-inject a small amount of high-reactivity diesel (near 20%) into the cylinder early in the compression stroke, and then a high-proportion n-butanol is introduced into the diesel atmosphere around -50 °CA ATDC. However, the situation for mid load is just opposite, where a high proportion of n-butanol is partially premixed in advance near -120 °CA, followed by a late diesel injection at -50 °CA ATDC. For high-load conditions, n-butanol still needs to be partially premixed in advance, while the diesel injection event is delayed after TDC, and the whole combustion presents a two-stage heat release feature.

(2) In the optimal low-load $DI^2$ strategy, the late n-butanol injection helps to increase the local equivalence ratio to avoid overly lean combustion, while the diesel injected early can be more evenly distributed in the cylinder, thus ensuring the fuel near the cylinder wall and the combustion chamber center also has sufficient reactivity to be completely oxidized. Both factors facilitate further improving the combustion efficiency at low load. For the mid load, the distribution of the pre-injected n-butanol before ignition is fairly even due to the sufficient mixing time and good fuel vaporization, and the homogeneity of the fuel/air mixture is significantly enhanced, which benefits to increase the fuel economy and achieve low engine noise and $NO_x$ emissions. As for the high load, two-stage combustion is utilized, and the diesel injection after TDC helps to increase engine output and IMEP, and reduce the fuel reactivity during the auto-ignition period, so that premature ignition and high pressure rise rate can be avoided.

(3) The ignition at low load is dominated by the temperature and fuel reactivity distributions in the cylinder. For the mid load, the fuel ignition is mainly driven by fuel reactivity. As for the high load condition, the ignition only

depends on the partially premixed n-butanol, and the fuel ignition is dominated by the in-cylinder temperature.

(4) Under low load conditions, the early injected diesel first participates in the fuel reaction and has an important effect on the in-cylinder thermal atmosphere promotion and active species accumulation before ignition. It is found that the pre-injected diesel is necessary to stabilize the ignition of the late-injected low-reactivity n-butanol. By adjusting the ratio of the high-reactivity diesel, ignition timing and combustion phasing can achieve a nearly fast linear response.

(5) For the low-load $DI^2$ combustion, compared with diesel, the n-butanol injection event is more important. The premature or too-late n-butanol injection leads to deteriorated fuel efficiency, especially for the B-SOI timing earlier than -70 °CA ATDC. Also, $NO_x$ emissions and the butanol injection timing at low load are positively correlated. For the mid load, the optimal diesel injection timing is limited to a narrow range of -50 to -20 °CA due to the RI and combustion efficiency constraints. For high load, a later D-SOI helps to smooth the heat release process and achieve lower pressure rise rate and $NO_x$ emissions while maintaining engine output power.

Overall, the current work shows that the ignition and performance of the dual-fuel $DI^2$ engine under a wide load range are highly dependent on the degree of the in-cylinder fuel-air mixing and the spatial distribution and stratification state of the dual fuel. Therefore, considering the significant effect of the fuel volatility and reactivity on the in-cylinder process of $DI^2$, the selection of the optimal fuel combination should be an important direction for future $DI^2$ research.

# Acknowledgements

The work was financially supported by the National Key Research and Development Program of China (Grand No. 2022YFE0199600).

# References

[1] Jones DT, Woods DR. Acetone-butanol fermentation revisited. Microbiol Rev 1986;50:484–524.

[2] Trindade WR da S, Santos RG dos. Review on the characteristics of butanol, its production and use as fuel in internal combustion engines. Renewable Sustainable Energy Rev 2017;69:642–51.

[3] Vinod Babu M, Madhu Murthy K, Amba Prasad Rao G. Butanol and pentanol: the promising biofuels for CI engines - a review. Renewable Sustainable Energy Rev 2017;78:1068–88.

[4] Green EM. Fermentative production of butanol-the industrial perspective. Curr Opin Biotechnol 2011;22:337–43.

[5] Li J, Zhang Y, Sun K, Liu W, Yan H, Meng J. Optimization of a cathodic electro-fermentation process for enhancing co-production of butanol and hydrogen via acetone-butanol-ethanol fermentation of Clostridium beijerinckii. Energy Convers Manage 2022;251:114987.

[6] Jin C, Yao M, Liu H, Lee CF, Ji J. Progress in the production and application of n-butanol as a biofuel. Renewable Sustainable Energy Rev 2011;15:4080–106.

[7] Zheng M, Han X, Asad U, Wang J. Investigation of butanol-fuelled HCCI combustion on a high efficiency diesel engine. Energy Convers Manage 2015;98:215–24.

[8] Zheng M, Li T, Han X. Direct injection of neat n-butanol for enabling clean low temperature combustion in a modern diesel engine. Fuel 2015;142:28–37.

[9] Doğan O. The influence of n-butanol/diesel fuel blends utilization on a small diesel engine performance and emissions. Fuel 2011;90:2467–72.

[10] Chen Z, Liu J, Han Z, Du B, Liu Y, Lee C. Study on performance and emissions of a passenger-car diesel engine fueled with butanol-diesel blends. Energy 2013;55:638–46.

[11] Rakopoulos DC, Rakopoulos CD, Giakoumis EG, Dimaratos AM, Kyritsis DC. Effects of butanol-diesel fuel blends on the performance and emissions of a high-speed DI diesel engine. Energy Convers Manage 2010;51:1989–97.

[12] Wadumesthrige K, Ng K, Salley S. Properties of butanol-biodiesel-ULSD ternary mixtures. SAE Int J Fuels Lubr 2010;3:660–70.

[13] Benajes J, Molina S, García A, Belarte E, Vanvolsem M. An investigation on RCCI combustion in a heavy duty diesel engine using in-cylinder blending of diesel and gasoline fuels. Appl Therm Eng 2014;63:66–76.

[14] Wang Y, Yao M, Li T, Zhang W, Zheng Z. A parametric study for enabling reactivity controlled compression ignition (RCCI) operation in diesel engines at various engine loads. Appl Energy 2016;175:389–402.

[15] Li Y, Jia M, Liu Y, Xie M. Numerical study on the combustion and emission characteristics of a methanol/diesel reactivity controlled compression ignition (RCCI) engine. Appl Energy 2013;106:184–97.

[16] Li Y, Jia M, Chang Y, Liu Y, Xie M, Wang T, Zhou L. Parametric study and optimization of a RCCI (reactivity controlled compression ignition) engine fueled with methanol and diesel. Energy 2014;65:319–32.

[17] Yu S, Li L, Zheng M. n-Butanol reactivity modulation with early fuel injections for low NOx compression ignition combustion. Fuel 2019;242:243–54.

[18] Xiao J, Jia M, Chang Y, Li Y, Xu Z, Xu G, Liu H, Wang T. Numerical optimization and comparative study of n-butanol concentration stratification combustion and n-butanol/diesel reactivity stratification combustion for advanced compression ignition (CI) engine. Fuel 2018;213:83–97.

[19] Jafari B, Seddiq M, Mirsalim SM. Impacts of diesel injection timing and syngas fuel composition in a heavy-duty RCCI engine. Energy Convers Manage 2021;247:114759.

[20] Kousheshi N, Yari M, Paykani A, Saberi Mehr A, de la Fuente GF. Effect of syngas composition on the combustion and emissions characteristics of a syngas/diesel RCCI engine. Energies 2020;13:212.

[21] Kokjohn SL, Musculus MPB, Reitz RD. Evaluating temperature and fuel stratification for heat-release rate control in a reactivity-controlled compression-ignition engine using optical diagnostics and chemical kinetics modeling. Combust Flame 2015;162:2729–42.

[22] Kokjohn SL, Hanson RM, Splitter DA, Reitz RD. Fuel reactivity controlled compression ignition (RCCI): a pathway to controlled high-efficiency clean combustion. Int J Engine Res 2011;12:209–26.

[23] Splitter D, Wissink M, Kokjohn S, Reitz RD. Effect of compression ratio and piston geometry on RCCI load limits and efficiency. SAE Technical Paper 2021-01-0383, 2012.

[24] Macián V, Monsalve-Serrano J, Villalta D, Fogué-Robles Á. Extending the potential of the dual-mode dual-fuel combustion towards the prospective EURO VII emissions limits using gasoline and OMEx. Energy Convers Manage 2021;233:113927.

[25] Wissink M, Reitz RD. Direct dual fuel stratification, a path to combine the benefits of RCCI and PPC. SAE Int J Engines 2015;8:878–89.

[26] Florea R, Neely GD, Abidin Z, Miwa J. Efficiency and emissions characteristics of partially premixed dual-fuel combustion by co-direct injection of NG and diesel fuel ($DI^2$). SAE Technical Paper 2016-01-0779, 2016.

[27] Cai Y, Jia M, Xu G, Li Y, Wang T. Feasibility study of the combustion strategy of n-butanol/diesel dual direct injection ($DI^2$) in a compression-ignition engine. Fuel 2021;289:119865.

[28] Lim JH, Reitz RD. High load (21 bar IMEP) dual fuel RCCI combustion using dual direct injection. J Eng Gas Turbines Power 2014;136:101514.

[29] Neely GD, Florea R, Miwa J, Abidin Z. Efficiency and emissions characteristics of partially premixed dual-fuel combustion by co-direct injection of NG and diesel fuel ($DI^2$) - Part 2. SAE Technical Paper 2017-01-0766, 2017.

[30] Li Y, Jia M, Xu L, Bai X-S. Multiple-objective optimization of methanol/diesel dual-fuel engine at low loads: a comparison of reactivity controlled compression ignition (RCCI) and direct dual fuel stratification (DDFS) strategies. Fuel 2020;262:116673.

[31] Lim JH, Reitz R. Improving high efficiency reactivity controlled compression ignition combustion with diesel and gasoline direct injection. Proc Inst Mech Eng, Part D: J Automob Eng 2013;227:17–30.

[32] Deb K, Member A, Pratap A, Agarwal S, Meyarivan T. A fast and elitist multiobjective genetic algorithm: NSGA-II. IEEE Trans Evol Comput 2002;6:182–97.

[33] Amsden AA. KIVA-3V: a block-structured KIVA program for engines with vertical or canted valves. Los Alamos National Laboratory Technical Report, LA-13313-MS, USA, 1997.

[34] Wang B-L, Lee C-W, Reitz RD, Miles PC, Han Z. A generalized renormalization group turbulence model and its application to a light-duty diesel engine operating in a low-temperature combustion regime. Int J Engine Res 2013;14:279–92.

[35] Ricart LM, Reltz RD, Dec JE. Comparisons of diesel spray liquid penetration and vapor fuel distributions with in-cylinder optical measurements. J Eng Gas Turbines Power 2000;122:588–95.

[36] Suo S, Jia M, Liu H, Wang T. Development of a new hybrid stochastic/trajectory droplet collision model for spray simulations in internal combustion engines. Int J Multiphase Flow 2021;137:103581.

[37] Yi P, Long W, Jia M, Tian J, Li B. Development of a quasi-dimensional vaporization model for multi-component fuels focusing on forced convection and high temperature conditions. Int J Heat Mass Transfer 2016;97:130–45.

[38] Zhang Y, Jia M, Liu H, Xie M, Wang T, Zhou L. Development of a new spray/wall interaction model for diesel spray under PCCI-engine relevant conditions. Atomization Sprays 2014;24:41–80.

[39] Zhang Y, Jia M, Liu H, Xie M. Development of an improved liquid film model for spray/wall interaction under engine-relevant conditions. Int J Multiphase Flow 2016;79:74–87.

[40] Cao J, Jia M, Niu B, Chang Y, Xu Z, Liu H. Establishment of an improved heat transfer model based on an enhanced thermal wall function for internal combustion engines operated under different combustion modes. Energy Convers Manage 2019;195:748–59.

[41] Kee RJ, Rupley FM, Miller JA. Chemkin-II: A Fortran chemical kinetics package for the analysis of gas-phase chemical kinetics. Sandia National Laboratory Technical Report, SAND-89-8009, USA, 1989.

[42] Dempsey AB, Curran SJ, Wagner RM. A perspective on the range of gasoline compression ignition combustion strategies for high engine efficiency and low NOx and soot emissions: effects of in-cylinder fuel stratification. Int J Engine Res 2016;17:897–917.

[43] Jia M, Xie M, Wang T, Peng Z. The effect of injection timing and intake valve close timing on performance and emissions of diesel PCCI engine with a full engine cycle CFD simulation. Appl Energy 2011;88:2967–75.

[44] Chang Y, Jia M, Xiao J, Li Y, Fan W, Xie M. Construction of a skeletal mechanism for butanol isomers based on the decoupling methodology. Energy Convers Manage 2016;128:250–60.

[45] Chang Y, Jia M, Li Y, Xie M. Application of the optimized decoupling methodology for the construction of a skeletal primary reference fuel mechanism focusing on engine-relevant conditions. Front Mech Eng 2015;1:1–11.

[46] Chang Y, Jia M, Liu Y, Li Y, Xie M. Development of a new skeletal mechanism for n-decane oxidation under engine-relevant conditions based on a decoupling methodology. Combust Flame 2013;160:1315–32.

[47] Jia M, Peng ZJ, Xie MZ. Numerical investigation of soot reduction potentials with diesel homogeneous charge compression ignition combustion by an improved phenomenological soot model. Proc Inst Mech Eng, Part D: J Automob Eng 2009;223:395–412.

[48] Wissink ML. Direct injection for dual fuel stratification (DDFS): improving the control of heat release in advanced IC engine combustion strategies. PhD thesis, University of Wisconsin-Madison, USA, 2015.

[49] Li Z, Huang G, Zhang Y, Zhao W, Li J, He Z, Qian Y, Lu X. Dual fuel intelligent charge compression ignition (ICCI) combustion: efficient and clean combustion technology for compression ignition engines. Fuel 2020;279:118565.

[50] Ning L, Duan Q, Kou H, Zeng K. Parametric study on effects of methanol injection timing and methanol substitution percentage on combustion and emissions of methanol/diesel dual-fuel direct injection engine at full load. Fuel 2020;279:118424.

[51] Long W, Li B, Cao J, Meng X, Tian J, Cui J, Tian H. Effects of dual-direct injection parameters on performance of fuel Jet Controlled Compression Ignition mode on a high-speed light duty engine. Fuel 2019;235:658–69.

[52] Liu X, Srna A, Yip HL, Kook S, Chan QN, Hawkes ER. Performance and emissions of hydrogen-diesel dual direct injection (H2DDI) in a single-cylinder compression-ignition engine. Int J Hydrogen Energy 2021;46:1302–14.

[53] Dong Y, Kaario O, Hassan G, Ranta O, Larmi M, Johansson B. High-pressure direct injection of methanol and pilot diesel: a non-premixed dual-fuel engine concept. Fuel 2020;277:117932.

[54] Brown BS. High-pressure direct-injection of natural gas with entrained diesel into a compression-ignition Engine. PhD thesis, University of British Columbia, Canada, 2008.

[55] McTaggart-Cowan G, Mann K, Huang J, Singh A, Patychuk B, Zheng Z, Munshi S. Direct injection of natural gas at up to 600 bar in a pilot-ignited heavy-duty engine. SAE Int J Engines 2015;8:981–96.

[56] Wärtsilä. Wärtsilä 34DF product guide. Finland, 2020. Retrieved from https://www.wartsila.com/marine/products/engines-and-generating-sets/dual-fuel-engines/wartsila-34df.

[57] Li Z, Wang Y, Yin Z, Gao Z, Wang Y, Zhen X. Parametric study of a single-channel diesel/methanol dual-fuel injector on a diesel engine fueled with directly injected methanol and pilot diesel. Fuel 2021;302:121156.

[58] Lim JH. High power output operation of RCCI combustion. PhD thesis, University of Wisconsin-Madison, USA, 2015.

[59] Jeftic M, Yang Z, Reader GT, Zheng M. Fuel efficiency analysis and peak pressure rise rate improvement for neat n-butanol injection strategies. Proc Inst Mech Eng, Part D: J Automob Eng 2017;231:50–65.

[60] Eng JA. Characterization of pressure waves in HCCI combustion. SAE Technical Paper 2002-01-2859, 2002.

[61] Xu G, Jia M, Li Y, Chang Y, Wang T. Potential of reactivity controlled compression ignition (RCCI) combustion coupled with variable valve timing (VVT) strategy for meeting Euro 6 emission regulations and high fuel efficiency in a heavy-duty diesel engine. Energy Convers Manage 2018;171:683–98.

[62] Desantes JM, Benajes J, García A, Monsalve-Serrano J. The role of the in-cylinder gas temperature and oxygen concentration over low load reactivity controlled compression ignition combustion efficiency. Energy 2014;78:854–68.

[63] Duan H, Jia M, Li Y, Wang T. A comparative study on the performance of partially premixed combustion (PPC), reactivity-controlled compression ignition (RCCI), and RCCI with reverse reactivity stratification (R-RCCI) fueled with gasoline and polyoxymethylene dimethyl ethers (PODEn). Fuel 2021;298:120838.

[64] Lu X, Ji L, Ma J, Zhou X, Huang Z. Combustion characteristics and influential factors of isooctane active-thermal atmosphere combustion assisted by two-stage reaction of n-heptane. Combust Flame 2011;158:203–16.

[65] Babajimopoulos A, Assanis DN, Flowers DL, Aceves SM, Hessel RP. A fully coupled computational fluid dynamics and multi-zone model with detailed chemical kinetics for the simulation of premixed charge compression ignition engines. Int J Engine Res 2005;6:497–512.